


Mantle data imply a decline of oxidizable volcanic gases could have triggered the Great Oxidation

Shintaro Kadoya ^{1✉}, David C. Catling ¹, Robert W. Nicklas², Igor S. Puchtel³ & Ariel D. Anbar⁴

Aerobic lifeforms, including humans, thrive because of abundant atmospheric O₂, but for much of Earth history O₂ levels were low. Even after evidence for oxygenic photosynthesis appeared, the atmosphere remained anoxic for hundreds of millions of years until the ~2.4 Ga Great Oxidation Event. The delay of atmospheric oxygenation and its timing remain poorly understood. Two recent studies reveal that the mantle gradually oxidized from the Archean onwards, leading to speculation that such oxidation enabled atmospheric oxygenation. But whether this mechanism works has not been quantitatively examined. Here, we show that these data imply that reducing Archean volcanic gases could have prevented atmospheric O₂ from accumulating until ^{oxygenation occurred by or after} ~2.5 Ga with ≥95% probability. For two decades, mantle oxidation has been dismissed as a key driver of the evolution of O₂ and aerobic life. Our findings warrant a reconsideration for Earth and Earth-like exoplanets.

¹Department of Earth and Space Sciences/Cross-Campus Astrobiology Program, University of Washington, Box 351310, Seattle, WA 98195-1310, USA.

²Geoscience Research Division, Scripps Institution of Oceanography, La Jolla, CA 92093, USA. ³Department of Geology, University of Maryland, College Park, MD 20742, USA. ⁴School of Earth and Space Exploration and School of Molecular Sciences, Arizona State University, Tempe, AZ 85287, USA.

✉email: shintaro.kadoya@gmail.com

The geological record of mass-independent sulfur isotope fractionation shows that O₂ first inundated the atmosphere during the Great Oxidation Event (GOE) between 2.4 and 2.1 Ga¹. However, redox-sensitive iron and molybdenum isotope data suggest the presence of O₂ in the 3.2–3.0-Ga marine photic zone^{2,3}, which implies that O₂-producing cyanobacteria existed long before the GOE. Indeed, models show that, under a globally anoxic atmosphere, cyanobacteria-derived O₂ produces photic zone oxygen oases^{4,5}. Geological data also indicate the presence of methanotrophy and oxidative nitrogen cycling in Neoproterozoic oceans and lakes, which suggest that O₂ was oxidizing sulfides and ammonium to make sulfate and nitrate, respectively^{6–8}. Such inferences are consistent with phylogenetic interpretations that oxygenic photosynthesis evolved by the mid-Archean [e.g., ref. ⁹]. In addition, paleoredox proxies suggest O₂ transients at 2.5 Ga^{6,7,10–16}, and point to the possibility of pervasive oxygenation of the oceans over continental margins^{17,18}.

The reasons for the delay of oxygenation of the atmosphere for hundreds of millions of years after the advent of oxygenic photosynthesis remain unknown. Numerous hypotheses rely on the notion that the atmospheric O₂ level is determined by a kinetic balance between O₂ supply and consumption^{19–23}. If the rapid and efficient O₂ sinks are larger than the O₂ supply, there are excess reductants, and the atmosphere remains anoxic even in the presence of global oxygenic photosynthesis. Rapid sinks include net reactions of O₂ with reducing gases emanating from the solid Earth, e.g., H₂, CO, H₂S, SO₂, and CH₄.

One possibility is that an increase in O₂ fluxes overwhelmed the efficient O₂ sinks, causing the GOE. However, the available data are not particularly persuasive. Photosynthetic O₂ production is accompanied by organic matter (CH₂O) in the net reaction CO₂ + H₂O = CH₂O + O₂. Because respiration or oxidative decay reverse this reaction (presently in ~50 years), the long-term net flux of O₂ occurs when organic matter is segregated from O₂ and buried.

Long-term changes in the burial rate of organic matter—and hence in the net supply of O₂—can be inferred from C isotopes in sedimentary rocks. Organic matter concentrates ¹²C relative to ¹³C, leaving marine inorganic carbonate ¹²C depleted; as such, carbon isotopes in marine carbonates and kerogens track f_{org} , the fraction of total carbon buried as organic matter. Isotopic mass balance shows little difference between the average organic burial fraction for 3.6–2.5 Ga of $f_{\text{org}} = 0.15 \pm 0.02$ [2 standard deviations (SD)] and that for 1.8–1.0 Ga of $f_{\text{org}} = 0.18 \pm 0.02$ [2 SD]²⁴, suggesting no significant increase in O₂ flux.

Of course, the inferred organic burial fraction and associated O₂ flux depend on assumptions about the carbon cycle. Challenges to a conventional carbon mass balance model include ¹²C-enriched carbon sequestered into seafloor carbonates²⁵ or into authigenic carbonates²⁶, or isotopic weathering inputs that scaled with the amount of atmospheric O₂^{24,27,28}. The first two hypotheses lack supporting evidence: Archean seafloor carbonate is not isotopically lighter than typical marine sedimentary carbonates²⁹, and the abundance of authigenic carbonates is low before the GOE compared with afterward³⁰, and is relatively small today³¹. The third idea is plausible: the lack of oxidative weathering in the Archean could modulate f_{org} ²⁷. However, the average organic content of Archean sedimentary rocks (3.59 wt%) is indistinguishable from that of Proterozoic (3.56 wt%)²⁴, and the cumulative distribution of total organic content in organic-rich Archean sedimentary rocks is identical to that of Neogene rocks¹.

Here we are interested in examining the potential implications of the trend in mantle redox state on the GOE. A lower Archean O₂ flux may be a possible factor, but that is not the focus of this paper.

Because f_{org} changed little with a conventional carbon cycle model, it has been proposed that a secular decline of efficient O₂ sinks, rather than an increase in f_{org} , caused the tipping point that initiated the GOE; this point would have been reached when the efficient O₂ sink flux fell below the organic burial flux of O₂^{19,22,32,33}. Models show that atmospheric O₂ would then rapidly accumulate, until oxidative weathering of the continents became a significant sink, causing O₂ concentrations to level off³⁴. Proxies suggest that the O₂ level, however, was still far below today's atmospheric O₂ concentrations [e.g., ref. ³⁵].

Qualitatively, the pre-GOE O₂ sink flux could have declined if the mantle's oxidation state increased over time^{32,36,37}. The proportion of reducing gases in volcanic emissions depends inversely on the oxygen fugacity (f_{O_2}) in their magma source region, the upper mantle. Thus, if the Archean mantle's f_{O_2} was low, the H₂/H₂O and CO/CO₂ ratios in Archean volcanic gases would have been high, suppressing atmospheric O₂ levels.

Until recently, studies suggested that the mantle's f_{O_2} had been similar to the modern value since at least the early Archean^{38–42}. The mantle f_{O_2} estimated by many of these studies has uncertainties that vary between ~1 log₁₀ unit^{38,43} and ~2 log₁₀ units^{41,42}. Changes in the oxygen fugacity of the mantle as small as ~0.5 log₁₀ units have been suggested to have a significant effect on atmospheric redox evolution³²; therefore, prior results do not preclude involvement in the GOE.

A notable study of mantle redox evolution is Li and Lee⁴⁰, who used the V/Sc ratios of a large database of primitive basalts to report that mantle oxidation state had not changed by more than 0.3 log₁₀ units since the Archean. The use of the V/Sc oxybarometer on large amounts of published basalt data relies upon the assumption that all of the studied basalts are the result of similar degrees of partial melting, and that they sample a spinel peridotite source with a primitive mantle V/Sc of ~5. None of these are necessarily safe assumptions. Average degree of partial melting was likely higher in the Archean due to higher mantle potential temperature. In addition, not all of the studied basalts were likely generated from melting of spinel peridotite, and residual garnet can have a potentially strong effect on V/Sc⁴⁴. Finally, the mantle sources of basalts vary greatly in the degree of previous melt depletion, and remelting of a previously depleted source can generate a low V/Sc melt and an erroneously reduced f_{O_2} . For all these reasons, the conclusions and quoted uncertainties of Li and Lee⁴⁰ must come into question.

Two new studies reveal an f_{O_2} trend. Aulbach and Stagno⁴⁵ carefully filtered V/Sc data to only include Archean basalts formed in a mid-ocean ridge (MOR)-like environment, while Nicklas et al.⁴⁶ calculated the f_{O_2} of ultramafic lavas directly without making assumptions about their source compositions. These new data, shown in Fig. 1a, indicate that mantle f_{O_2} increased by ~1.3 log₁₀ units from the early Archean to Proterozoic, and likely represent the current best estimate for mantle redox evolution.

Both datasets in Fig. 1a show a similar f_{O_2} trend, but each dataset was determined using a different oxybarometer. The f_{O_2} derived from different oxybarometers shows a systematic offset, the reason for which is currently unclear, as oxybarometry performed using different methods on modern rocks gives values that vary outside of analytical uncertainty⁴⁷. One possible explanation involves the degassing of volatile species, such as SO₂, which have the potential to strongly reduce a lava shortly prior to eruption⁴⁸. Degassing may lead to an offset between these two datasets because the V-partitioning oxybarometer of Nicklas et al.⁴⁶ measures the f_{O_2} of komatiites and picrites, while the V/Sc ratio oxybarometer of Aulbach and Stagno⁴⁵ infers the f_{O_2} of basalts and picrites. Komatiites are high-temperature, high-degree

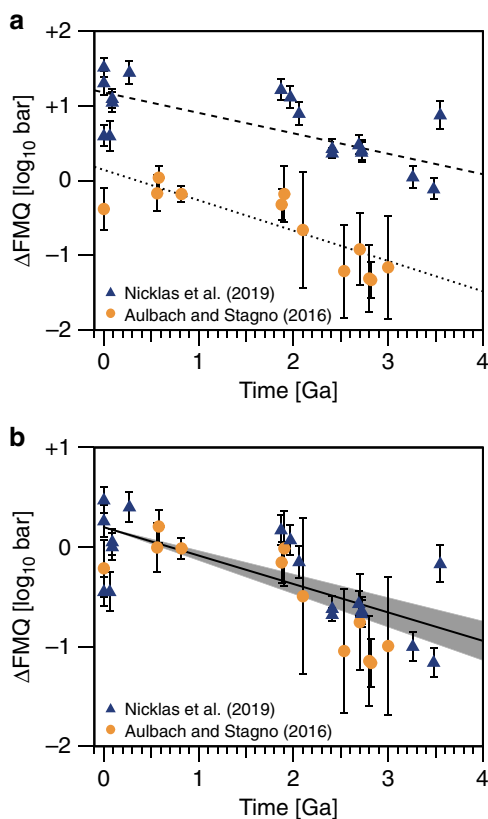


Fig. 1 Evolution of the oxygen fugacity of mantle. The oxygen fugacity (f_{O_2}) is in \log_{10} units relative to the Fayalite–Magnetite–Quartz (FMQ) buffer. In **a**, we show original data of Aulbach and Stagno⁴⁵ and Nicklas et al.⁴⁶. Dotted and dashed lines in **a** represent a linear fit for the data of Aulbach and Stagno⁴⁵ and Nicklas et al.⁴⁶, respectively, showing similar trends. Both datasets should converge on an average modern f_{O_2} value inferred from mid-ocean ridge basalt (MORB). So, in **b**, we anchor the datasets to the MORB-inferred f_{O_2} of the modern mantle, 0.2^{50} . Thus, 0.2 is added to Aulbach and Stagno data⁴⁵ and -1.00 to Nicklas et al. data⁴⁶. The black solid line and gray shaded region in **b** represent the median value and 95% confidence interval of oxygen fugacity, respectively. The error bar represents uncertainty of 1σ . The gray shaded region corresponds to a variation of the slope of the linear fit, which is propagated from the variations of the samples (i.e., the error bars). Note that in **b**, the variation of the f_{O_2} of the modern mantle, which is discussed later, is neglected.

partial melts that are undersaturated in sulfur, while basalts are lower-degree, sulfur-saturated melts. Hence, sulfur degasses more from basaltic lavas than komatiitic lavas, i.e., decreases the f_{O_2} of basalts more than that of komatiite⁴⁶.

As each mantle oxidation trend only compares samples analyzed by the same oxybarometry method, and each study also analyzed modern mid-ocean ridge basalt (MORB) with its respective method, we can anchor each trend to the current canonical modern MORB value of $+0.2 \pm 0.3 \log_{10}$ units above the fayalite–magnetite–quartz (FMQ) buffer as determined by X-ray absorption near-edge spectroscopy^{49,50}. Upon anchoring, the two mantle oxidation trends overlap within their respective uncertainties, lending credence to the idea of mantle oxidation (Fig. 1b).

Although it has been speculated that the secular trends in the mantle f_{O_2} in Fig. 1a and the timing of the GOE may be related^{45,46}, this hypothesis has never been quantitatively tested in a redox model for the surface environment using data-derived trends of f_{org} and mantle f_{O_2} .

In this study, we show that the new data imply that reducing Archean volcanic gases would prevent atmospheric O_2 from accumulating, and then the GOE would occur by or after ~ 2.5 Ga with $\geq 95\%$ probability. Thus, we conclude that secular oxidation of the mantle have indeed triggered oxygenation of the atmosphere.

Results

Oxygenation parameter. We evaluate whether the atmosphere was prone to oxygenation at any given time using an oxygenation parameter, K_{oxy} ^{22,33,34}. This parameter is the ratio of O_2 source fluxes to kinetically efficient O_2 sink fluxes, which we consider here to be dominated by oxidizable volcanic gases

$$K_{\text{oxy}} \equiv \frac{\text{O}_2 \text{ source fluxes}}{\text{non-weathering O}_2 \text{ sink fluxes (may incl. excess reductants)}}. \quad (1)$$

Fluxes are quantified in units of $\text{T mol O}_2 \text{ yr}^{-1}$. When $K_{\text{oxy}} < 1$, gaseous volcanic O_2 sinks exceed O_2 sources, and excess H_2 builds up until balanced by escape to space. When $K_{\text{oxy}} > 1$, O_2 sources exceed efficient O_2 sinks, and O_2 builds up until balanced by oxidative weathering. Box modeling coupled to photochemistry shows that $K_{\text{oxy}} = 1$ defines the point when the atmosphere becomes oxidic (see Fig. 7b of Claire et al.³⁴). For detailed information, see the “Methods” section and the Supplementary information.

Evolution of the oxygenation parameter. As an initial, illustrative trial, we took the organic burial fraction (f_{org}) to be constant at 20%, which is a canonical value adopted by previous researchers [e.g., refs. 21,32], to isolate the effect of the secular change in mantle f_{O_2} shown in Fig. 1b. As shown in Fig. 2a, the results are that the oxygenation parameter (K_{oxy}) monotonically increases with time.

In Fig. 2a, K_{oxy} larger than unity occurs when the production of O_2 via organic burial and deposition of pyrite (i.e., the numerator of Eq. (20)) exceeds the consumption of O_2 from oxidizable volcanic gases (i.e., the denominator of Eq. (20)). Then atmospheric O_2 accumulates, and oxidative weathering kicks in and balances the excess O_2 production^{22,33,34}. In contrast, when K_{oxy} is smaller than unity, the production of O_2 via organic burial and deposition of pyrite (i.e., the numerator of Eq. (20)) is smaller than the consumption of O_2 by reducing volcanic gases (i.e., the denominator of Eq. (20)). Under such a condition, atmospheric O_2 cannot accumulate, and the buildup of excess of reducing gases, such as CH_4 and H_2 , is limited by their decomposition in the upper atmosphere and the escape of hydrogen to space^{22,33,34}.

The 5% probability quantile of K_{oxy} (the lower end of gray shaded region) crosses unity (a dotted gray line) at 2.62 Ga in the purely illustrative case of Fig. 2a. This means that at 2.62 Ga and later, the probability that K_{oxy} is larger than unity, allowing atmospheric oxygenation, is 95% or more. Hereafter, we designate this 95% threshold as the oxidic transition time.

In Eq. (20), K_{oxy} also depends on f_{org} , which has fluctuated over time. In Fig. 2b, which we subsequently call our standard case, we included temporal changes in f_{org} from Krissansen-Totton et al.²⁴ derived from the carbon isotope record (Supplementary Fig. 1). Unlike in Fig. 2a, K_{oxy} fluctuates in Fig. 2b because of fluctuations in f_{org} derived from the carbon isotope record. However, K_{oxy} still increases with time. Here, the oxidic transition time of this standard case is 2.48 Ga, which is delayed because of relatively low values of f_{org} before 2.5 Ga (Supplementary Fig. 1). Hence, even when we include temporal changes of f_{org} , the atmosphere still becomes oxidic at 2.48 Ga (or afterward) with 95% (or more) probability.

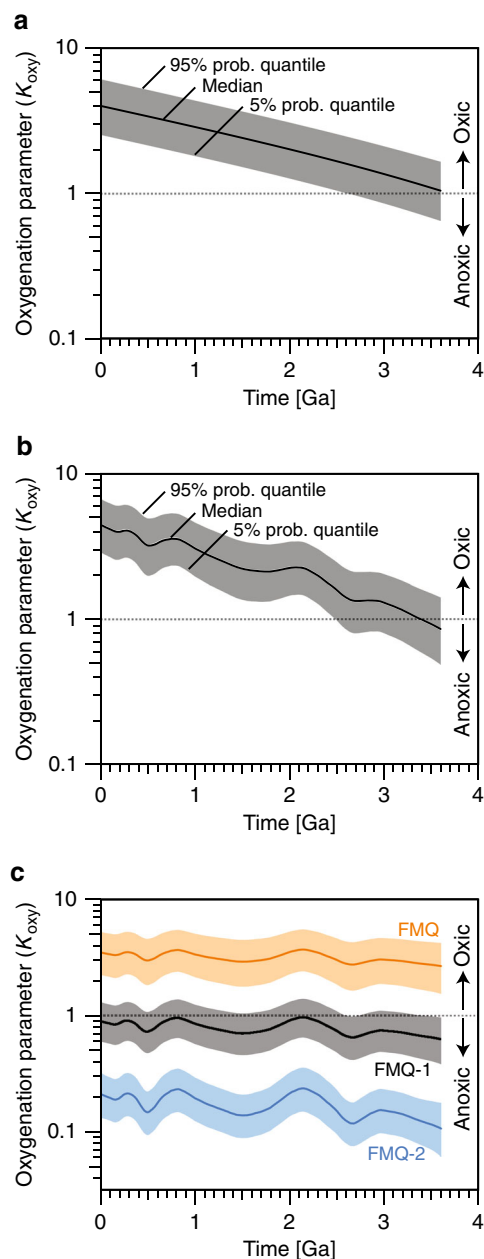


Fig. 2 Evolution of the dimensionless oxygenation parameter, K_{oxy} . Solid lines represent median values, and the shaded region bounds 5% to 95% probability quantiles. These are obtained by 10,000 times Monte-Carlo simulations. Gray dotted lines highlight $K_{\text{oxy}} = 1$, above which the atmosphere is oxic; otherwise, it is anoxic. **a** Organic burial fraction is constant at 20%, and the secular increase in the oxygen fugacity of mantle in Fig. 1b is considered. **b** Both a change in organic burial fraction from Krissansen-Totton et al.²⁴ and secular increase in the oxygen fugacity in Fig. 1b are considered. **c** Oxygen fugacity is assumed to be constant at three different levels (blue: FMQ-2, black: FMQ-1, orange: FMQ). The fluctuations come from imposed changes in organic burial fraction. In **b**, the parameter K_{oxy} exceeds unity by ~2.5 Ga with $\geq 95\%$ probability.

On the other hand, the probability of $K_{\text{oxy}} > 1$ is less than 50% before 3.38 Ga, for example, 30% at 3.6 Ga (Fig. 2b, see also Supplementary Fig. 2). This indicates that the atmosphere was likely reducing in the early Archean despite the possible presence of oxygenic photosynthesis. Thus, the increase in f_{O_2} of the mantle would cause the atmosphere to shift from reducing to oxic, and the shift seemed to occur before ~2.5 Ga.

For comparison, we also did calculations for three hypothetical scenarios where the mantle f_{O_2} was fixed at FMQ-2, FMQ-1, and FMQ (Fig. 2c). We also included temporal fluctuations in f_{org} , as in Fig. 2b, which are reflected in the fluctuations of K_{oxy} . In these scenarios, an oxic transition for K_{oxy} does not occur, although K_{oxy} occasionally becomes greater than 1 in the FMQ-1 case within the gray shaded region of uncertainty in Fig. 2c. Thus, the transitions from $K_{\text{oxy}} < 1$ to $K_{\text{oxy}} > 1$ in Fig. 2a, b are mainly due to the temporal increase in mantle f_{O_2} taken from the fit in Fig. 1.

Discussion

As shown above, an empirically-inferred increase in mantle f_{O_2} causes an increase in K_{oxy} , resulting in the shift of the atmosphere from reducing to oxic (Fig. 2). However, this result does not exclude a role for other processes in the oxidation of the atmosphere as explained below.

The result of the standard case shows that uncertainties in the f_{O_2} time series and the oxygen flux estimates from the carbon isotope record propagate through the calculations, so that the uncertainty envelope allows an oxic regime even before ~2.5 Ga (Fig. 2b). On the other hand, geological evidence, such as mass-independent sulfur isotope fractionation¹, indicates an anoxic atmosphere for the Archean Earth before 2.4–2.3 Ga though a recent study suggests that the GOE occurred somewhat earlier than 2.4 Ga⁵¹. This discrepancy in the timing of the GOE might also be caused by not considering other processes that may delay the oxic transition.

To investigate the effect of processes proposed by previous studies^{20–22,27,52,53}, we did some sensitivity studies and obtained the same trends as previous studies. As explained in Supplementary Note 1, K_{oxy} decreases if the degassing pressure is high, if the carbon and/or sulfur degassing fluxes are low, and/or if the rate of magnetite deposition via serpentinization is high, which generates oxidizable hydrogen that is a sink for O_2 .

If K_{oxy} was lower, the atmosphere in the early Archean would be more reducing, and the oxic transition time would be delayed, because of the following processes: a secular decrease in the degassing pressure due to a transition from submarine to sub-aerial volcanism [e.g., refs. 20,52], a secular increase in the carbon and/or sulfur degassing due to an increase in their continent and/or ocean floor reservoir²¹, and/or a secular decrease in the magnetite deposition flux via serpentinization, which might result from a decrease in the degree of partial melting of the mantle caused by secular cooling²². The magnitude of the Archean serpentinization flux of H_2 is debated, since it is only significant today from slow-spreading centers where ultramafic rocks are exposed⁵³.

There is another possible process that contributed to the delay in the oxic transition along with slow mantle oxidation. Because of the lack of oxidative weathering in the Archean, the carbon isotope input into the atmosphere-ocean could have been relatively heavy compared with mantle values, and so less organic burial was needed for the mass balance²⁷.

We also investigated the uncertainty of the anchoring value of the mantle f_{O_2} evolution (Supplementary Note 1). For the standard case (Fig. 2), we modeled the evolution of the mantle f_{O_2} anchoring the trend to the average f_{O_2} of modern MORB, i.e., $\Delta\text{FMQ}_0 = +0.2$ [see also Eq. (4)]⁵⁰. However, this reference value has an uncertainty of $0.3 \log_{10}$ units⁵⁰. Anchoring the f_{O_2} trend to a lower ΔFMQ_0 value causes lower mantle f_{O_2} in the past, resulting in a more reducing atmosphere in the Archean and delaying the oxic transition time (Supplementary Fig. 8).

Thus, all of the processes discussed in the preceding three paragraphs might affect the GOE's timing and so are potentially complicating factors.

Observations show that erupted volcanic gas is more oxidized, i.e., has a larger ΔFMQ , than its source melt^{54,55}. The relative oxidative state of the volcanic gas results from reactions within a closed gas mixture due to cooling^{54,55}. Consequently, it has been proposed that secular cooling of the mantle could have facilitated the GOE⁵⁵. Also, observations seem to indicate that it is not possible to calculate the oxidation effect, i.e., K_{oxy} , of the volcanic gas using the ΔFMQ of its source, although we did this in this study. However, the assumptions of these previous studies^{54,55} need to be reconsidered, as follows.

Recent work⁵⁶ discusses how cooling affects the oxidation state and the K_{oxy} of a volcanic gas mixture considering two stages of degassing, i.e., the stage where volcanic gas is buffered by its source melt (melt-buffered stage), and the stage where the volcanic gas is a closed system (closed stage). For the closed stage, the same conclusion was reached as in the previous studies^{54,55}, i.e., cooling increases ΔFMQ of a closed volcanic gas compared with that of its source melt. However, in a closed gas mixture, oxidation of a gas should be accompanied by a reduction of another gas, so any reaction in the closed gas mixture does not change the overall O_2 sink in the gas mixture⁵⁶. Hence, to evaluate the K_{oxy} of volcanic gas, we can neglect the effect of reactions after the volcanic gas separated from its source, i.e., the observed difference in the oxidation state between erupted volcanic gas and its source melt.

For the melt-buffered stage, cooling results in reduction of a gas mixture and a decrease in K_{oxy} if the ΔFMQ of the source melt is buffered and constant⁵⁶. This is because cooling decreases the absolute value of f_{O_2} of the FMQ buffer (Supplementary Fig. 4). A trend of smaller K_{oxy} with lower mantle temperature is shown in Supplementary Fig. 3a. However, the oxic transition time is insensitive to temperature if the temperature is higher than the solidus temperature of dry peridotite ($\sim 1390\text{ K}$)⁵⁷, as shown in Supplementary Fig. 3b. The mantle temperature in the Archean would be between 1600 and 1900 K [e.g., refs. 57–59]. Hence, the secular cooling of the mantle would affect less the GOE.

Note that Holland's f number [e.g., ref. 32] was used in Moussallam et al.⁴⁸, while K_{oxy} was used in Kadoya et al.⁵⁶. However, the temperature dependence of Holland's f number is essentially the same as that of K_{oxy} . This point is explained in Supplementary Note 2.

A decrease in mantle temperature might delay the oxic transition time if the temperature was lower than the solidus temperature of dry peridotite (Supplementary Fig. 3b). Degassing would occur under such a low temperature in arc volcanism because the hydrous phase of the subducted crust can lower the melting temperature [e.g., ref. 60]. However, the island arc basalts are often more oxidized than the mid-ocean ridge basalts or oceanic island basalts⁶¹. Hence, we cannot conclude that arc volcanism, whose degassing temperature would be low, delayed the oxic transition time.

A question might arise about our assumption that the f_{O_2} of the volcanic gas was equal to that of the upper mantle. Degassing can reduce the source melt, e.g., SO_2 degassing⁴⁸. However, during the melt-buffer stage, i.e., when the volcanic gas mixture interacts with the ambient melt, the f_{O_2} of the gas will be equal to that of the melt. In addition, during the closed stage, i.e., after the gas mixture decouples from the ambient melt, any reaction within the gas mixture does not change the oxygenation effect of the gas⁵⁶. Thus, the oxygenation effect of the gas should be examined using the f_{O_2} of the gas when the gas decouples from the melt. Also, at that time, the f_{O_2} of the gas would equal to that of the ambient melt, which has already experienced degassing. Therefore, we can calculate K_{oxy} using the f_{O_2} from the Archean that is anchored today to modern MORB f_{O_2} .

It is also noteworthy that the similar trend of the mantle f_{O_2} with time is observed by the measurement of f_{O_2} of different rocks^{46,59}. This similarity indicates that the increase in f_{O_2} of melts follows the same trend of the decreasing mantle f_{O_2} with time, despite the difference in the degree of partial melting, which also supports our assumption that the f_{O_2} of the volcanic gas increased with time.

The assumption of the anchoring value of the f_{O_2} bears consideration. In this study, we anchored the f_{O_2} of the volcanic gas and the melt at the value of the modern MORB, implicitly assuming that the f_{O_2} of the melt does not change after the melt decouples from the gas. However, if the f_{O_2} of the melt changes after the decoupling from the gas, it also changes the timing of the GOE as indicated by the parameter study of the anchoring value of the f_{O_2} (Supplementary Fig. 8).

Of course, a major question is what drove the increase in mantle f_{O_2} and, hence, could have driven the GOE. One possibility is that convection-driven homogenization of an initially redox-stratified primordial mantle was responsible for this change^{45,46,62}. The basic idea is that in the early deep mantle, Fe^{2+} disproportionated to Fe^{3+} and Fe metal due to high pressure. The latter was lost to the core, leaving a more oxidized lower mantle below a relatively reduced upper mantle. According to Andraut et al.⁶², the primitive mantle contained excess of Fe^{3+} corresponding to $\sim 60\%$ of an ocean's worth of oxygen.

However, another possible driver of upper mantle oxidation has recently gained evidence in its favor. Ancient air dissolved in inclusions of seawater in Archean quartz shows that the nine isotopes of Xe become increasingly isotopically heavy throughout the Archean and early Proterozoic until the GOE⁶³. The most plausible explanation is a very rapid escape of hydrogen to space that dragged along ionized Xe atoms, which would have fractionated Xe isotopes because of mass-dependent escape⁶⁴.

Substantial loss of a strong reducing agent, i.e., hydrogen, would have oxidized the Earth, with the oxidation affecting the reservoir from which the hydrogen originated. Thus, the mantle would become gradually more oxidized because the hydrogen comes from the decomposition of water in volcanic melts, schematically represented as $3\text{FeO} + \text{H}_2\text{O} \rightarrow \text{Fe}_3\text{O}_4 + \text{H}_2$. The upper mantle (down to $\sim 660\text{-km}$ depth) contains the equivalent of $\sim 20\%$ of an ocean's worth of oxygen as Fe^{3+} [ref. 65, p. 207]. The Xe isotope data require Archean hydrogen loss from the equivalent of $\sim 10\%$ of an ocean⁶⁴. Thus, if the f_{O_2} trend in Fig. 1b explains the GOE, as shown in Fig. 2b, the f_{O_2} trend, in turn, may have been driven by hydrogen escaping to space from the Earth's pre-GOE anoxic atmosphere [e.g., refs. 19,66].

Hydrogen escape as a mechanism for mantle oxidation³⁶ has been proposed previously, but has been rejected over the last two decades because of reports of seemingly constant mantle f_{O_2} through time^{39,67,68}. Our results suggest that this mechanism may need to be reconsidered.

In summary, we examined whether new data for increasing mantle oxygen fugacity (f_{O_2}) since the Archean could explain the GOE, when O_2 first accumulated in the Earth's atmosphere. The onset of the GOE can only be properly quantified by considering sources and sinks of oxygen in a global redox balance of the surface environment. The oxygenation parameter K_{oxy} used for this purpose is defined as the ratio of O_2 sources to kinetically rapid sinks. For an anoxic atmosphere, $K_{\text{oxy}} < 1$, while for an oxic atmosphere, $K_{\text{oxy}} > 1$; by evaluating when $K_{\text{oxy}} = 1$, we determined how mantle f_{O_2} trends affected the onset of the GOE.

A more reducing mantle with low f_{O_2} produces a greater proportion of reducing volcanic gases. So, we found that the data-derived trend of mantle f_{O_2} likely prevented O_2 building up in the atmosphere with relatively high probability ($\sim 70\%$ at 3.6 Ga) and

caused an oxic transition from $K_{\text{oxy}} < 1$ to $K_{\text{oxy}} > 1$ with >95% probability after 2.5 Ga.

Our calculated timing of the GOE is relatively insensitive to the mantle potential temperature, but depends on the assumed degassing pressure, and total outgassing fluxes of carbon and sulfur relative to total hydrogen. An additional oxidative sink of ferric iron in magnetite deposition has a minor effect, unless this flux in the Archean exceeded ten times the modern flux.

If a trend in mantle f_{O_2} controlled the timing of the GOE, then the cause of mantle oxidation is ultimately important for setting the tempo of biological evolution because macroscopic, energy-intensive aerobic life was impossible when O_2 levels were negligible. Possible drivers of mantle redox evolution are the mixing of a redox heterogeneous mantle or the time-integrated oxidative effect of the breakdown of mantle water in volcanism, and the escape of hydrogen to space. Such processes could also apply to other Earth-like planets elsewhere, and would thus determine whether such planets could be habitats for complex aerobic life with high O_2 demand⁶⁹.

Methods

The redox tipping point of the atmosphere can only be quantified by considering the global redox flux balance of the early atmosphere and ocean, which is as fundamental as mass or energy conservation^{22,65}, p. 221–223].

To evaluate the redox tipping point of the atmosphere, we use the oxygenation parameter, K_{oxy} , which is the ratio of the O_2 source fluxes (F_{oxi}) to non-weathering O_2 sink fluxes (F_{red})^{22,34,69}:

$$K_{\text{oxy}} \equiv \frac{F_{\text{oxi}}}{F_{\text{red}}} \quad (2)$$

The fluxes, F_{oxi} and F_{red} , are calculated using fluxes of volcanic gas, such as CO and SO_2 , organic burial flux, and pyrite burial flux. In the subsequent sections, we will describe a model of each flux, and then explain models of F_{oxi} and F_{red} .

Fluxes related to source and sink of oxygen. In this section, we explain the components, which are used to calculate the O_2 source (F_{oxi}) and a kinetically rapid sink of O_2 (F_{red}). For the calculation of F_{oxi} and F_{red} , see the next section.

Hydrogen is degassed to the ocean–atmosphere system as hydrogen molecules (H_2), water vapor (H_2O), methane (CH_4), and hydrogen sulfide (H_2S). Accordingly, a total flux of hydrogen (F_{hydrogen}) can be expressed as follows:

$$F_{\text{hydrogen}} = F_{\text{H}_2} + F_{\text{H}_2\text{O}} + 2F_{\text{CH}_4} + F_{\text{H}_2\text{S}}, \quad (3)$$

where F_x is a flux of x . Methane contains the equivalent of two H_2 molecules, so F_{CH_4} is weighted by a factor of 2.

Carbon is degassed to the ocean–atmosphere system as carbon dioxide (CO_2), carbon monoxide (CO), and methane (CH_4), and deposited as organic matter (org) and carbonate (carb). Since we assume that carbon is in a steady state, the total flux of carbon (F_{carbon}) is equal to input and output fluxes, which can be expressed as follows:

$$F_{\text{carbon}} \equiv F_{\text{CO}_2} + F_{\text{CO}} + F_{\text{CH}_4} = F_{\text{org}} + F_{\text{carb}}, \quad (4)$$

where F_x is a flux of x as in Eq. (3).

The ratio of the organic burial to the total carbon flux (i.e., $f_{\text{org}} = F_{\text{carb}}/F_{\text{carbon}}$) can be evaluated using the geological record of carbon isotopes in organic and inorganic carbon [e.g., ref. 24]. Supplementary Fig. 1 shows the temporal change in the f_{org} , which is derived by Krissansen-Totton et al.²⁴.

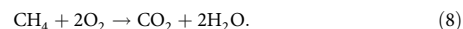
Similarly, sulfur (S) is degassed to the ocean–atmosphere system as sulfur dioxide (SO_2) and hydrogen sulfide (H_2S), and deposited as pyrite (FeS_2) and sulfate (e.g., CaSO_4). However, we neglect the deposition of sulfate because we focus on the Archean eon, the surface environment was anoxic, and there was very little sulfate (~2.5 μM , i.e., 0.01% of modern level) in the Archean ocean^{70,71}. Since we assume that sulfur is in steady state, a total flux of sulfur (F_{sulfur}) is equal to input and output fluxes, which can be expressed as follows:

$$F_{\text{sulfur}} \equiv F_{\text{SO}_2} + F_{\text{H}_2\text{S}} = \frac{1}{2}F_{\text{FeS}_2}, \quad (5)$$

where F_x is a flux of x as in Eq. (3).

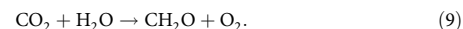
Sources and sinks of oxygen. In this section, we explain models of the O_2 source (F_{oxi}) and a kinetically rapid sink of O_2 (F_{red}), which are used for the calculation of K_{oxy} (Eq. (2)).

We take H_2O and CO_2 to be redox-neutral, so hydrogen (H_2), carbon monoxide (CO), and methane (CH_4) are sinks of oxygen, as follows:



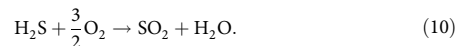
Hence, one mole of H_2 degassing corresponds to 0.5 mole of O_2 consumption. Similarly, one mole of CO and CH_4 degassing corresponds to 0.5 and 2 moles of O_2 consumption, respectively.

On the other hand, the burial of organic matter (CH_2O) is a source of oxygen, as follows:

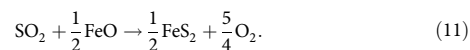


Hence, one mole of the burial of organic matter corresponds to one mole of O_2 production.

We also assume that SO_2 is redox-neutral, so H_2S is a sink of oxygen, as follows:



Also, reduction of SO_2 must work as a source of oxygen, as follows:



Hence, one mole of SO_2 degassing corresponds to 1.25 mole of O_2 production. On the other hand, one mole of H_2S degassing corresponds to 0.25 mole of O_2 consumption.

As explained above, degassing of H_2 , CO , CH_4 , and H_2S is a sink of oxygen. Accordingly, F_{red} is expressed as follows:

$$F_{\text{red}} = \frac{1}{2}F_{\text{H}_2} + \frac{1}{2}F_{\text{CO}} + 2F_{\text{CH}_4} + \frac{1}{4}F_{\text{H}_2\text{S}}. \quad (12)$$

On the other hand, burial of organic matter and SO_2 degassing are sources of oxygen. Accordingly, F_{oxi} is expressed as follows:

$$F_{\text{oxi}} = F_{\text{org}} + \frac{5}{4}F_{\text{SO}_2}. \quad (13)$$

Derivation of oxygenation parameter. Substituting Eqs. (12) and (13) into Eq. (2), K_{oxy} is rewritten as follows:

$$K_{\text{oxy}} = \frac{4F_{\text{org}} + 5F_{\text{SO}_2}}{2F_{\text{H}_2} + 2F_{\text{CO}} + 8F_{\text{CH}_4} + F_{\text{H}_2\text{S}}}. \quad (14)$$

We now define χ_c and χ_s as follows:

$$\chi_c \equiv \frac{F_{\text{carbon}}}{F_{\text{hydrogen}}}, \quad \chi_s \equiv \frac{F_{\text{sulfur}}}{F_{\text{hydrogen}}}. \quad (15)$$

In addition, we define r_{H_2} as the ratio of a flux of hydrogen molecule to a total flux of hydrogen:

$$r_{\text{H}_2} \equiv \frac{F_{\text{H}_2}}{F_{\text{hydrogen}}}. \quad (16)$$

Similarly, we defined the following parameters:

$$r_{\text{CO}} \equiv \frac{F_{\text{CO}}}{F_{\text{carbon}}}, \quad r_{\text{CH}_4} \equiv \frac{F_{\text{CH}_4}}{F_{\text{carbon}}}, \quad f_{\text{org}} \equiv \frac{F_{\text{org}}}{F_{\text{carbon}}}, \quad (17)$$

$$r_{\text{SO}_2} \equiv \frac{F_{\text{SO}_2}}{F_{\text{sulfur}}}, \quad r_{\text{H}_2\text{S}} \equiv \frac{F_{\text{H}_2\text{S}}}{F_{\text{sulfur}}}. \quad (18)$$

If we substitute from the above for the various gas fluxes and flux of organic burial, Eq. (14) can be rewritten as

$$K_{\text{oxy}} = \frac{4f_{\text{org}}F_{\text{carbon}} + 5r_{\text{SO}_2}F_{\text{sulfur}}}{2r_{\text{H}_2}F_{\text{hydrogen}} + (2r_{\text{CO}} + 8r_{\text{CH}_4})F_{\text{carbon}} + r_{\text{H}_2\text{S}}F_{\text{sulfur}}}. \quad (19)$$

If we now divide the above equation by F_{hydrogen} , we arrive at the form

$$K_{\text{oxy}} = \frac{4f_{\text{org}}\chi_c + 5r_{\text{SO}_2}\chi_s}{2r_{\text{H}_2} + (2r_{\text{CO}} + 8r_{\text{CH}_4})\chi_c + r_{\text{H}_2\text{S}}\chi_s}. \quad (20)$$

Kasting²² argues that an additional O_2 flux, in the form of $F_{\text{Fe}_3\text{O}_4}$, could be included in the denominator of Eq. (2). If we take FeO as the redox reference state of iron for the Archean surface environment, then the formation of ferric iron in magnetite ($\text{Fe}_2^+\text{Fe}^{2+}\text{O}_4$) in iron formations or during serpentinization and its burial removes oxidizing power from the surface environment or, equivalently, is an input flux of reducing power. We initially neglect the deposition of magnetite, and then examine its specific influence later. When the magnetite deposition is

taken into account, K_{oxy} can be rewritten as

$$K_{\text{oxy}} = \frac{4f_{\text{org}}\chi_c + 5r_{\text{SO}_2}\chi_s}{2r_{\text{H}_2} + (2r_{\text{CO}} + 8r_{\text{CH}_4})\chi_c + r_{\text{H}_2\text{S}}\chi_s + \frac{F_{\text{Fe}_3\text{O}_4}}{F_{\text{hydrogen}}}}, \quad (21)$$

where $F_{\text{Fe}_3\text{O}_4}$ is an O_2 consumption via magnetite deposition in the unit of T mol $\text{O}_2 \text{ yr}^{-1}$. For example, the modern $F_{\text{Fe}_3\text{O}_4}$ is $0.05 \sim 0.2 \text{ T mol O}_2 \text{ yr}^{-1}$ ^{72,73}.

Equilibrium state of volcanic gases. In this section, we will explain how to calculate the flux ratios, i.e., r_x for each volatile species x in Eq. (20).

To calculate fluxes of volcanic gases, we first assume that equilibrium states are achieved for volcanic volatiles in the silicate melt:

$$\begin{cases} \text{H}_2\text{O} = \text{H}_2 + \frac{1}{2}\text{O}_2 \\ \text{CO}_2 = \text{CO} + \frac{1}{2}\text{O}_2 \\ \text{CO}_2 + 2\text{H}_2\text{O} = \text{CH}_4 + 2\text{O}_2 \\ \text{SO}_2 + \text{H}_2\text{O} = \text{H}_2\text{S} + \frac{3}{2}\text{O}_2 \end{cases} \quad (22)$$

These equations have equilibrium constants that are as follows, in terms of fugacities (f_x) for each volatile species x :

$$\begin{cases} K_1 = \frac{f_{\text{H}_2}f_{\text{O}_2}^{0.5}}{f_{\text{H}_2\text{O}}} \\ K_2 = \frac{f_{\text{CO}}f_{\text{O}_2}^{0.5}}{f_{\text{CO}_2}} \\ K_3 = \frac{f_{\text{CH}_4}f_{\text{O}_2}^3}{f_{\text{CO}_2}f_{\text{H}_2\text{O}}^2} \\ K_4 = \frac{f_{\text{H}_2\text{S}}f_{\text{O}_2}^{1.5}}{f_{\text{SO}_2}f_{\text{H}_2\text{O}}} \end{cases} \quad (23)$$

We assume that gas fluxes will be in proportion to their fugacities, e.g., $f_{\text{H}_2} = P_{\text{tot}} \times F_{\text{H}_2} / F_{\text{tot}}$. Here, P_{tot} is a total pressure under which degassing occurs. F_{tot} is a total degassing flux that can be written as

$$F_{\text{tot}} \approx F_{\text{H}_2\text{O}} + F_{\text{H}_2} + F_{\text{carbon}} + F_{\text{sulfur}}, \quad (24)$$

$$= F_{\text{hydrogen}} (r_{\text{H}_2\text{O}} + r_{\text{H}_2} + \chi_c + \chi_s). \quad (25)$$

Then, we obtain the following equations:

$$\begin{cases} \frac{K_1}{f_{\text{O}_2}^{0.5}} = \frac{r_{\text{H}_2}}{r_{\text{H}_2\text{O}}} \\ \frac{K_2}{f_{\text{O}_2}^{0.5}} = \frac{r_{\text{CO}}}{r_{\text{CO}_2}} \\ \frac{K_3}{f_{\text{O}_2}^3} p_{\text{tot}}^2 = \frac{r_{\text{CH}_4}}{r_{\text{CO}_2}} \left(\frac{r_{\text{H}_2\text{O}} + r_{\text{H}_2} + \chi_c + \chi_s}{r_{\text{H}_2\text{O}}} \right)^2 \\ \frac{K_4}{f_{\text{O}_2}^{1.5}} p_{\text{tot}} = \frac{r_{\text{H}_2\text{S}}}{r_{\text{SO}_2}} \times \frac{r_{\text{H}_2\text{O}} + r_{\text{H}_2} + \chi_c + \chi_s}{r_{\text{H}_2\text{O}}} \end{cases} \quad (26)$$

where f_{O_2} is an oxygen fugacity, which we will explain later. We calculate equilibrium constants of the above reactions using data of NIST⁷⁴. According to Eqs. (3)–(5), we also obtain the following equations:

$$\begin{cases} r_{\text{H}_2} + r_{\text{H}_2\text{O}} + 2r_{\text{CH}_4}\chi_c + r_{\text{H}_2\text{S}}\chi_s = 1 \\ r_{\text{CO}_2} + r_{\text{CO}} + r_{\text{CH}_4} = 1 \\ r_{\text{SO}_2} + r_{\text{H}_2\text{S}} = 1 \end{cases} \quad (27)$$

Hence, given mantle temperature, a total pressure, and oxygen fugacity in the mantle, and solving Eqs. (26) and (27), we obtain fluxes of each molecular species.

Hereafter, we explain how to solve Eqs. (26) and (27). First of all, we defined variables as follows:

$$A \equiv \frac{K_1}{f_{\text{O}_2}^{0.5}}, B \equiv \frac{K_2}{f_{\text{O}_2}^{0.5}}, C \equiv \frac{K_3}{f_{\text{O}_2}^3} p_{\text{tot}}^2, D \equiv \frac{K_4}{f_{\text{O}_2}^{1.5}} p_{\text{tot}},$$

$$r_{\text{tot}} \equiv (1 + A)r_{\text{H}_2\text{O}} + \chi_c + \chi_s.$$

Then, Eq. (27) can be rewritten as follows:

$$\begin{cases} (1 + A)r_{\text{H}_2\text{O}} + 2\chi_c C \left(\frac{r_{\text{H}_2\text{O}}}{r_{\text{tot}}} \right)^2 r_{\text{CO}_2} + \chi_s D \left(\frac{r_{\text{H}_2\text{O}}}{r_{\text{tot}}} \right) r_{\text{SO}_2} = 1 \\ r_{\text{CO}_2} + Br_{\text{CO}_2} + C \left(\frac{r_{\text{H}_2\text{O}}}{r_{\text{tot}}} \right)^2 r_{\text{CO}_2} = 1 \\ r_{\text{SO}_2} + D \left(\frac{r_{\text{H}_2\text{O}}}{r_{\text{tot}}} \right) r_{\text{SO}_2} = 1 \end{cases} \quad (28)$$

Hence,

$$r_{\text{CO}_2} = \frac{r_{\text{tot}}^2}{(1 + B)r_{\text{tot}}^2 + Cr_{\text{H}_2\text{O}}^2}, \quad (29)$$

$$r_{\text{SO}_2} = \frac{r_{\text{tot}}}{r_{\text{tot}} + Dr_{\text{H}_2\text{O}}}. \quad (30)$$

The unknown variable, $f_{\text{H}_2\text{O}}$, is obtained by solving the following equation:

$$(1 + A)r_{\text{H}_2\text{O}} + 2\chi_c \frac{Cr_{\text{H}_2\text{O}}^2}{(1 + B)r_{\text{tot}}^2 + Cr_{\text{H}_2\text{O}}^2} + \chi_s \frac{Dr_{\text{H}_2\text{O}}}{r_{\text{tot}} + Dr_{\text{H}_2\text{O}}} = 1. \quad (31)$$

Oxygen fugacity of mantle. As explained above, we need the oxygen fugacity, f_{O_2} , of volcanic gas to calculate the volcanic gas speciation. To evaluate the K_{oxy} of the gas, we can use the f_{O_2} of the source of the gas, i.e., the mantle melt⁵⁶. In addition, both experimental⁷⁵ and empirical data from natural samples⁷⁶ show that the mantle melt records the same f_{O_2} as its mantle residue, and therefore its mantle source. Hence, we evaluate the K_{oxy} using the f_{O_2} of the mantle.

According to Aulbach and Stagno⁴⁵ and Nicklas et al.⁴⁶, the oxygen fugacity of the mantle has increased by $+0.9 \pm 0.2$ [2 SD] in \log_{10} units during the past 3 Gyr. Since two independent datasets show the same trend, secular oxidation of the mantle is corroborated. In addition, the oxygen fugacity of the modern mantle is $+0.2 \pm 0.6$ [2 SD] in \log_{10} units above the FMQ buffer⁵⁰. Here, FMQ is the fayalite–magnetite–quartz synthetic buffer, which defines f_{O_2} at a particular temperature and pressure, e.g., $f_{\text{O}_2} = 10^{-8.5}$ bar at 1200 °C (1473.15 K and 0.5 MPa). Hence, we modeled the evolution of the mantle f_{O_2} in \log_{10} units above the FMQ buffer as follows:

$$\Delta\text{FMQ} = \Delta\text{FMQ}_0 + at. \quad (32)$$

where t is time in units of Ga, and the slope, a , is -0.29 ± 0.05 [2 SD] in units of per Ga. For the standard case, we set ΔFMQ_0 at 0.2 \log_{10} units⁵⁰, and later discuss the effect of the variation of this parameter.

Figure 1b shows the evolutionary range of oxygen fugacity for the standard case with its uncertainties. Further details for the comparison of the datasets of Fig. 1b are given in Supplementary Note 3.

Other input parameters. As indicated in Eqs. (30) and (31), the flux ratios, r_x in Eq. (20), depend on the total flux ratios of carbon and sulfur relative to hydrogen, χ_c and χ_s . In addition, the flux ratios also depend on the temperature and pressure of the system.

Initially, we assume modern values for the total flux ratios of carbon and sulfur relative to hydrogen. The modern total degassing fluxes of hydrogen, carbon, and sulfur (in all their forms) are 97 ± 20 , 9 ± 2 , and $2.2 \pm 0.7 \text{ T mol yr}^{-1}$, respectively [ref. 65, p. 203 and p. 221]. Hence, present-day $\chi_c = 0.1 \pm 0.03$ and $\chi_s = 0.023 \pm 0.0086$. Later, we examine the effect of these parameters on the results of our modeling.

Similarly, we use a modern mantle potential temperature of 1623.15 K (1350 °C)⁷⁷ and a pressure of 0.5 MPa⁷⁸ first. We examine the sensitivity to these parameters later.

Data availability

The datasets generated during the current study are available in the Zenodo repository [<https://doi.org/10.5281/zenodo.3668382>].

Code availability

The source code used in this study is also available in the Zenodo repository [<https://doi.org/10.5281/zenodo.3668382>].

Received: 15 October 2019; Accepted: 6 May 2020;

Published online: 02 June 2020

References

- Lyons, T. W., Reinhard, C. T. & Planavsky, N. J. The rise of oxygen in Earth's early ocean and atmosphere. *Nature* **506**, 307–315 (2014).
- Planavsky, N. J. et al. Evidence for oxygenic photosynthesis half a billion years before the Great Oxidation Event. *Nat. Geosci.* **7**, 283–286 (2014).
- Satkoshi, A. M., Beukes, N. J., Li, W. Q., Beard, B. L. & Johnson, C. M. A redox-stratified ocean 3.2 billion years ago. *Earth Planet. Sci. Lett.* **430**, 43–53 (2015).
- Kasting, J.F., Schopf, J.W. & Klein, C. Models relating to Proterozoic atmospheric and oceanic chemistry. in *The Proterozoic Biosphere: A Multidisciplinary Study* (eds Schopf, J. W. & Klein, C.) 1185–1187 (Cambridge University Press, Cambridge, 1992).
- Olson, S. L., Kump, L. R. & Kasting, J. F. Quantifying the areal extent and dissolved oxygen concentrations of Archean oxygen oases. *Chem. Geol.* **362**, 35–43 (2013).
- Godfrey, L. V. & Falkowski, P. G. The cycling and redox state of nitrogen in the Archean ocean. *Nat. Geosci.* **2**, 725–729 (2009).
- Garvin, J., Buick, R., Anbar, A. D., Arnold, G. L. & Kaufman, A. J. Isotopic evidence for an aerobic nitrogen cycle in the latest Archean. *Science* **323**, 1045–1048 (2009).

8. Stüeken, E. E. & Buick, R. Environmental control on microbial diversification and methane production in the Mesoarchean. *Precambrian Res.* **304**, 64–72 (2018).
9. Schirmer, B. E., Gugger, M. & Donoghue, P. C. J. Cyanobacteria and the Great Oxidation Event: evidence from genes and fossils. *Palaeontology* **58**, 769–785 (2015).
10. Kaufman, A. J. et al. Late Archean biospheric oxygenation and atmospheric evolution. *Science* **317**, 1900–1903 (2007).
11. Anbar, A. D. et al. A whiff of oxygen before the Great Oxidation Event? *Science* **317**, 1903–1906 (2007).
12. Reinhard, C. T., Raiswell, R., Scott, C., Anbar, A. D. & Lyons, T. W. A late Archean sulfidic sea stimulated by early oxidative weathering of the continents. *Science* **326**, 713–716 (2009).
13. Duan, Y. et al. Molybdenum isotope evidence for mild environmental oxygenation before the Great Oxidation Event. *Geochim. Cosmochim. Acta* **74**, 6655–6668 (2010).
14. Kendall, B., Brennecke, G. A., Weyer, S. & Anbar, A. D. Uranium isotope fractionation suggests oxidative uranium mobilization at 2.50 Ga. *Chem. Geol.* **362**, 105–114 (2013).
15. Kendall, B., Creaser, R. A., Reinhard, C. T., Lyons, T. W. & Anbar, A. D. Transient episodes of mild environmental oxygenation and oxidative continental weathering during the late Archean. *Sci. Adv.* **1**, e1500777 (2015).
16. Stüeken, E. E., Buick, R. & Anbar, A. D. Selenium isotopes support free O₂ in the latest Archean. *Geology* **43**, 259–262 (2015).
17. Kendall, B. et al. Pervasive oxygenation along late Archean ocean margins. *Nat. Geosci.* **3**, 647–652 (2010).
18. Ostrander, C. M. et al. Fully oxygenated water columns over continental shelves before the Great Oxidation Event. *Nat. Geosci.* **12**, 186–191 (2019).
19. Catling, D. C., Zahnle, K. J. & McKay, C. P. Biogenic methane, hydrogen escape, and the irreversible oxidation of early Earth. *Science* **293**, 839–843 (2001).
20. Kump, L. R. & Barley, M. E. Increased subaerial volcanism and the rise of atmospheric oxygen 2.5 billion years ago. *Nature* **448**, 1033–1036 (2007).
21. Holland, H. D. Why the atmosphere became oxygenated: a proposal. *Geochim. Cosmochim. Acta* **73**, 5241–5255 (2009).
22. Kasting, J. F. What caused the rise of atmospheric O₂? *Chem. Geol.* **362**, 13–25 (2013).
23. Lee, C. T. A. et al. Two-step rise of atmospheric oxygen linked to the growth of continents. *Nat. Geosci.* **9**, 417–424 (2016).
24. Krissansen-Totton, J., Buick, R. & Catling, D. C. A statistical analysis of the carbon isotope record from the Archean to Phanerozoic and implications for the rise of oxygen. *Am. J. Sci.* **315**, 275–316 (2015).
25. Bjerrum, C. J. & Canfield, D. E. New insights into the burial history of organic carbon on the early Earth. *Geochem. Geophys. Geosyst.* **5**, Q08001 (2004).
26. Schrag, D. P. Authigenic carbonate and the history of the global carbon cycle. *Science* **339**, 1383–1383 (2013).
27. Derry, L. A. Organic carbon cycling and the lithosphere. in *Treatise on Geochemistry* (Second Edition) (eds. Holland, H. D. & Turekian, K. K.) 239–249 (Elsevier, Oxford, 2014).
28. Daines, S. J., Mills, B. J. W. & Lenton, T. M. Atmospheric oxygen regulation at low proterozoic levels by incomplete oxidative weathering of sedimentary organic carbon. *Nat. Commun.* **8**, 14379 (2017).
29. Nakamura, K. & Kato, Y. Carbonatization of oceanic crust by the seafloor hydrothermal activity and its significance as a CO₂ sink in the early archaean. *Geochim. Cosmochim. Acta* **68**, 4595–4618 (2004).
30. Fallick, A. E., Melezhik, V. A. & Simonson, B. M. The ancient anoxic biosphere was not as we know it. in *Biosphere Origin and Evolution* (eds. Dobretsov, N., Kolchanov, N., Rozanov, A., & Zavarzin, G.) 169–188 (Springer US, Boston, MA, 2008).
31. Sun, X. L. & Turchyn, A. V. Significant contribution of authigenic carbonate to marine carbon burial. *Nat. Geosci.* **7**, 201–204 (2014).
32. Holland, H. D. Volcanic gases, black smokers, and the Great Oxidation Event. *Geochim. Cosmochim. Acta* **66**, 3811–3826 (2002).
33. Catling, D. C. & Claire, M. W. How Earth's atmosphere evolved to an oxic state: a status report. *Earth Planet. Sci. Lett.* **237**, 1–20 (2005).
34. Claire, M. W., Catling, D. C. & Zahnle, K. J. Biogeochemical modelling of the rise in atmospheric oxygen. *Geobiology* **4**, 239–269 (2006).
35. Planavsky, N. J. et al. A case for low atmospheric oxygen levels during Earth's middle history. *Emerg. Top. Life Sci.* **2**, 149–159 (2018).
36. Kasting, J. F., Egger, D. H. & Raeburn, S. P. Mantle redox evolution and the oxidation state of the Archean atmosphere. *J. Geol.* **101**, 245–257 (1993).
37. Kump, L. R., Kasting, J. F. & Barley, M. E. Rise of atmospheric oxygen and the "upside-down" Archean mantle. *Geochem. Geophys. Geosyst.* **2**, 2000GC000114 (2001).
38. Canil, D. Vanadium partitioning and the oxidation state of archaean komatiite magmas. *Nature* **389**, 842–845 (1997).
39. Delano, J. W. Redox history of the Earth's interior: implications for the origin of life. *Orig. Life Evol. Biosph.* **31**, 311–341 (2001).
40. Li, Z.-X. A. & Lee, C.-T. A. The constancy of upper mantle fO₂ through time inferred from V/Sc ratios in basalts. *Earth Planet. Sci. Lett.* **228**, 483–493 (2004).
41. Trail, D., Watson, E. B. & Tailby, N. D. The oxidation state of Hadean magmas and implications for early Earth's atmosphere. *Nature* **480**, 79–82 (2011).
42. Rollinson, H., Adetunji, J., Lenaz, D. & Szilas, K. Archaean chromitites show constant Fe³⁺/Fe in Earth's asthenospheric mantle since 3.8 Ga. *Lithos* **282**, 316–325 (2017).
43. Canil, D. & Fedortchouk, Y. Olivine-liquid partitioning of vanadium and other trace elements, with applications to modern and ancient picrites. *Can. Mineral.* **39**, 319–330 (2001).
44. Wang, J. et al. Oxidation state of arc mantle revealed by partitioning of V, Sc, and Ti between mantle minerals and basaltic melts. *J. Geophys. Res.* **124**, 4617–4638 (2019).
45. Aulbach, S. & Stagno, V. Evidence for a reducing Archean ambient mantle and its effects on the carbon cycle. *Geology* **44**, 751–754 (2016).
46. Nicklas, R. W. et al. Secular mantle oxidation across the Archean-Proterozoic boundary: Evidence from V partitioning in komatiites and picrites. *Geochim. Cosmochim. Acta* **250**, 49–75 (2019).
47. Mallmann, G. & O'Neill, H. S. Calibration of an empirical thermometer and oxybarometer based on the partitioning of Sc, Y and V between olivine and silicate melt. *J. Petrol.* **54**, 933–949 (2013).
48. Moussallam, Y. et al. The impact of degassing on the oxidation state of basaltic magmas: a case study of Kilauea volcano. *Earth Planet. Sci. Lett.* **450**, 317–325 (2016).
49. Berry, A. J., Stewart, G. A., O'Neill, H. S. C., Mallmann, G. & Mosselmans, J. F. W. A re-assessment of the oxidation state of iron in MORB glasses. *Earth Planet. Sci. Lett.* **483**, 114–123 (2018).
50. O'Neill, H. S. C., Berry, A. J. & Mallmann, G. The oxidation state of iron in mid-ocean ridge basaltic (MORB) glasses: implications for their petrogenesis and oxygen fugacities. *Earth Planet. Sci. Lett.* **504**, 152–162 (2018).
51. Philippot, P. et al. Globally asynchronous sulphur isotope signals require re-definition of the Great Oxidation Event. *Nat. Commun.* **9**, 1–10 (2018).
52. Gaillard, F., Scaillet, B. & Arndt, N. T. Atmospheric oxygenation caused by a change in volcanic degassing pressure. *Nature* **478**, 229–233 (2011).
53. Keir, R. S. A note on the fluxes of abiogenic methane and hydrogen from mid-ocean ridges. *Geophys. Res. Lett.* **37**, L24609 (2010).
54. Oppenheimer, C. et al. Influence of eruptive style on volcanic gas emission chemistry and temperature. *Nat. Geosci.* **11**, 678–681 (2018).
55. Moussallam, Y., Oppenheimer, C. & Scaillet, B. On the relationship between oxidation state and temperature of volcanic gas emissions. *Earth Planet. Sci. Lett.* **520**, 260–267 (2019).
56. Kadoya, S., Catling, D. C., Nicklas, R. W., Puchtel, I. S. & Anbar, A. D. Mantle cooling causes more reducing volcanic gases and gradual reduction of the atmosphere. *Geochem. Perspect. Lett.* **13**, 25–29 (2020).
57. Hirschmann, M. M. Mantle solidus: experimental constraints and the effects of peridotite composition. *Geochem. Geophys. Geosyst.* **1**, 2000GC000070 (2000).
58. Nisbet, E. G., Cheadle, M. J., Arndt, N. T. & Bickle, M. Constraining the potential temperature of the Archean mantle—a review of the evidence from komatiites. *Lithos* **30**, 291–307 (1993).
59. Aulbach, S. & Arndt, N. T. Eclogites as palaeodynamic archives: evidence for warm (not hot) and depleted (but heterogeneous) Archean ambient mantle. *Earth Planet. Sci. Lett.* **505**, 162–172 (2019).
60. Till, C. B., Grove, T. L. & Withers, A. C. The beginnings of hydrous mantle wedge melting. *Contrib. Mineral. Petrol.* **163**, 669–688 (2012).
61. Carmichael, I. S. E. The redox states of basic and silicic magmas: a reflection of their source regions? *Contrib. Mineral. Petrol.* **106**, 129–141 (1991).
62. Andrault, D. et al. Large oxygen excess in the primitive mantle could be the source of the great oxygenation event. *Geochem. Perspect. Lett.* **6**, 5–10 (2018).
63. Avce, G. et al. Evolution of atmospheric xenon and other noble gases inferred from Archean to Paleoproterozoic rocks. *Geochim. Cosmochim. Acta* **232**, 82–100 (2018).
64. Zahnle, K. J., Gacesa, M. & Catling, D. C. Strange messenger: a new history of hydrogen on Earth, as told by xenon. *Geochim. Cosmochim. Acta* **244**, 56–85 (2019).
65. Catling, D. C. & Kasting, J. F. *Atmospheric Evolution on Inhabited and Lifeless Worlds*. (Cambridge University Press, New York, 2017).
66. Zahnle, K. J. & Catling, D. C. Waiting for oxygen. in *Special Paper 504: Early Earth's Atmosphere and Surface Environment* (eds. Shaw, G. H.) 37–48 (Geological Society of America, Boulder, 2014).
67. Canil, D. Vanadium in peridotites, mantle redox and tectonic environments: Archean to present. *Earth Planet. Sci. Lett.* **195**, 75–90 (2002).
68. Lee, C. T. A., Leeman, W. P., Canil, D. & Li, Z. X. A. Similar V/Sc systematics in morb and arc basalts: implications for the oxygen fugacities of their mantle source regions. *J. Petrol.* **46**, 2313–2336 (2005).
69. Catling, D. C., Glein, C. R., Zahnle, K. J. & McKay, C. P. Why O₂ is required by complex life on habitable planets and the concept of planetary "oxygenation time". *Astrobiology* **5**, 415–438 (2005).

70. Canfield, D. E., Habicht, K. S. & Thamdrup, B. The Archean sulfur cycle and the early history of atmospheric oxygen. *Science* **288**, 658–661 (2000).
71. Crowe, S. A. et al. Sulfate was a trace constituent of Archean seawater. *Science* **346**, 735–739 (2014).
72. Sleep, N.H. Dioxygen over geologic time. in *Metal Ions in Biological Systems, Vol. 43, Biogeochemical Cycles of Elements* (eds. Sigel, H. & Sigel, R.) 49–73 (Taylor & Francis, Boca Raton, FL, 2005).
73. Canfield, D. E., Rosing, M. T. & Bjerrum, C. Early anaerobic metabolisms. *Philos. Trans. R. Soc. B* **361**, 1819–1834 (2006).
74. Chase, M.W. *NIST-JANAF thermochemical tables*, Fourth edition (American Institute of Physics, 1998).
75. Davis, F. A. & Cottrell, E. Experimental investigation of basalt and peridotite oxybarometers: Implications for spinel thermodynamic models and Fe³⁺ compatibility during generation of upper mantle melts. *Am. Mineral.* **103**, 1056–1067 (2018).
76. Birner, S. K., Cottrell, E., Warren, J. M., Kelley, K. A. & Davis, F. A. Peridotites and basalts reveal broad congruence between two independent records of mantle fo₂ despite local redox heterogeneity. *Earth Planet. Sci. Lett.* **494**, 172–189 (2018).
77. Herzberg, C., Condie, K. & Korenaga, J. Thermal history of the Earth and its petrological expression. *Earth Planet. Sci. Lett.* **292**, 79–88 (2010).
78. Holland, H.D. *The Chemical Evolution of the Atmosphere and Oceans*. (Princeton University Press, Princeton, 1984).

Acknowledgements

Funding support came from NSF Frontiers in Earth System Dynamics award No. 1338810.

Author contributions

D.C.C. designed the study. S.K. performed the calculation and data analysis. S.K. with D. C.C. wrote the paper with input from R.W.N., I.S.P., and A.D.A. All authors discussed the results and commented on the paper.

Competing interests

The authors declare no competing interests.

Additional information

Supplementary information is available for this paper at <https://doi.org/10.1038/s41467-020-16493-1>.

Correspondence and requests for materials should be addressed to S.K.

Peer review information *Nature Communications* thanks Bruno Scaillet and the other, anonymous, reviewer(s) for their contribution to the peer review of this work. Peer reviewer reports are available.

Reprints and permission information is available at <http://www.nature.com/reprints>

Publisher's note Springer Nature remains neutral with regard to jurisdictional claims in published maps and institutional affiliations.



Open Access This article is licensed under a Creative Commons Attribution 4.0 International License, which permits use, sharing, adaptation, distribution and reproduction in any medium or format, as long as you give appropriate credit to the original author(s) and the source, provide a link to the Creative Commons license, and indicate if changes were made. The images or other third party material in this article are included in the article's Creative Commons license, unless indicated otherwise in a credit line to the material. If material is not included in the article's Creative Commons license and your intended use is not permitted by statutory regulation or exceeds the permitted use, you will need to obtain permission directly from the copyright holder. To view a copy of this license, visit <http://creativecommons.org/licenses/by/4.0/>.

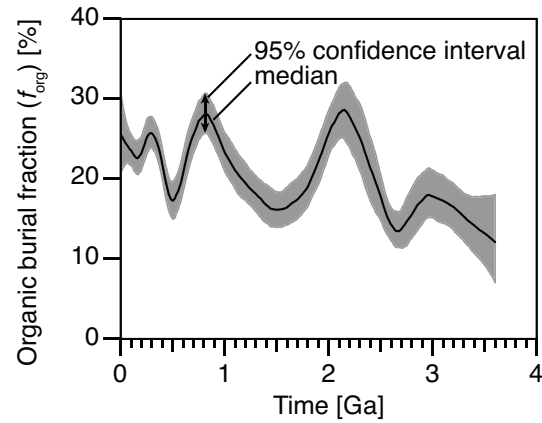
© The Author(s) 2020

Supplementary Information for
“Mantle data imply
a decline of oxidizable volcanic gases
could have triggered the Great Oxidation”

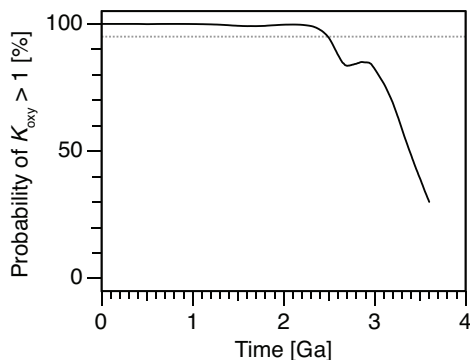
Shintaro Kadoya¹, David C. Catling¹,
Robert W. Nickal², Igor S. Puchtel³ & Ariel D. Anbar⁴

1. Department of Earth and Space Sciences/ cross-campus Astrobiology Program, University of Washington
2. Geoscience Research Division, Scripps Institution of Oceanography
3. Department of Geology, University of Maryland
4. School of Earth and Space Exploration and School of Molecular Sciences, Arizona State University

Supplementary Figures



Supplementary Figure 1: Evolution of organic burial fraction (f_{org}) based on Krissansen-Totton et al. [1]. This diagram corresponds to the case of the locally weighted scatterplot smoothing (LOWESS) in Fig. 3C of Krissansen-Totton et al. [1]. The black solid line and gray shaded region represents the median value and 95% confidence interval, respectively.



Supplementary Figure 2: Probability that the oxygenation parameter (K_{oxy}) is larger than unity ($P(K_{\text{oxy}} > 1)$) as a function of time. The black solid line represents the $P(K_{\text{oxy}} > 1)$ for the standard case (See also Fig.2b). The $P(K_{\text{oxy}} > 1)$ tends to increase with time, which corresponds to the increase in K_{oxy} (See also Fig.2b). The $P(K_{\text{oxy}} > 1)$ is 95% (the gray dotted line) at 2.4 Ga, which is the oxic transition time.

Supplementary Notes

Supplementary Note 1: Sensitivity test

In the main text, we assumed that the mantle temperature, degassing pressure, and the total flux ratio of carbon and sulfur (i.e., χ_c and χ_s in Equation 15), were constant. We also neglected the deposition of magnetite and the uncertainty of the oxygen fugacity of the modern mantle. Here, we examined the sensitivity of our results to changes in these parameters.

As a consequence of the sensitivity tests, we generally obtained trends consistent with previous works. As explained below, the mantle temperature has little effect on the oxic transition time (Supplementary Figure 3). On the other hand, a degassing pressure much higher than assumed in the standard case can affect the oxic transition time (Supplementary Figure 5). The oxic transition time may also be sensitive to other parameters: factors related to sedimentary recycling of carbon and sulfur (χ_c and χ_s) as shown in Supplementary Figure 6, the deposition flux of magnetite (Supplementary Figure 7), and the oxygen fugacity that is assumed for the modern mantle (Supplementary Figure 8).

1.1 Mantle temperature

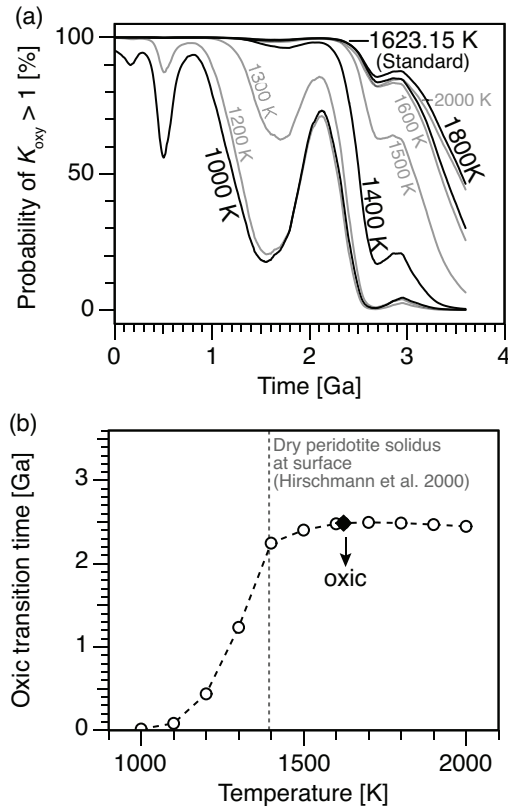
For our standard case (Fig. 2b), we assumed a mantle temperature of 1623.15 K, i.e., the modern potential temperature of the mantle [2]. In contrast, [3] estimated the modern redox proportions of volcanic gases using a temperature of 1473.15 K. However, it is likely that the potential temperature of the Archean mantle was higher today [e.g., 2, 4, 5]. On the other hand, the temperature for the gas vented from volcanic arcs would be lower than the mantle potential temperature because hydration associated with subduction would decrease the melt temperature, resulting in low degassing temperature. Hence, we calculated K_{oxy} with different temperatures (Supplementary Figure 3). In each calculation, we kept the mantle temperature constant and did not consider mantle cooling.

Supplementary Figure 3a shows the evolutions of $P(K_{\text{oxy}} > 1)$ for different temperatures. As shown in Supplementary Figure 3a, higher temperature tends to result in higher $P(K_{\text{oxy}} > 1)$, i.e., larger K_{oxy} . This is because an absolute value of oxygen fugacity of the mantle, f_{O_2} , decreases with a decrease in the temperature. Here, note that the oxidation state of the mantle is represented as $\Delta\text{FMQ} \equiv \log_{10} f_{\text{O}_2} - \log_{10} f_{\text{O}_2, \text{FMQ}}$, where $f_{\text{O}_2, \text{FMQ}}$ is the oxygen fugacity of the fayalite-magnetite-quartz buffer (see also Fig. 1). Since the $f_{\text{O}_2, \text{FMQ}}$ decreases with the decrease in temperature (Supplementary Figure 4), the f_{O_2} of source melt, and therefore, f_{O_2} of the volcanic gas do decrease with the cooling even if ΔFMQ is constant. So, lower temperature results in more reducing volcanic gas (Supplementary Figure 3a).

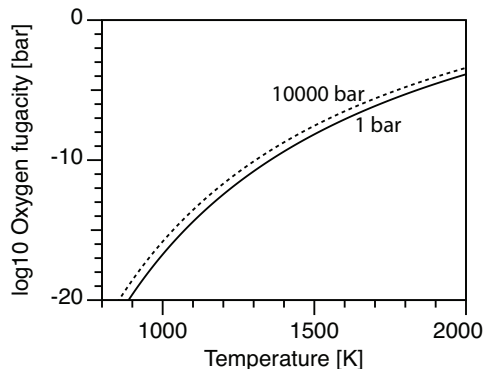
Supplementary Figure 3b shows the oxic transition time for different temperatures. As explained above, cooling causes a decrease in K_{oxy} (Supplementary Figure 3a), the cooling also decreases the oxic transition time (Supplementary Figure 3a). However, such temperature dependence of volcanic gas is relatively weak and not significant for a mantle temperature exceeding 1400 K (Supplementary Figure 3a).

Given that cooling of the potential temperature of the mantle from 1900 K to 1600 K [e.g., 2, 4, 5], the hot mantle in the early Archean tends to cause a relatively high possibility of $K_{\text{oxy}} > 1$, i.e., of the oxic atmosphere (Supplementary Figure 3a). However, the oxic transition time does not change so much (Supplementary Figure 3b).

On the other hand, arc volcanism seems to decrease the K_{oxy} (Supplementary Figure 3a) and the oxic transition time (Supplementary Figure 3b) considering that the hydrous phases within the oceanic crust lower the melt-



Supplementary Figure 3: A sensitivity study for mantle temperature: (a) probability that the oxygenation parameter is larger than unity ($P(K_{\text{oxy}} > 1)$) as a function of time, and (b) an oxic transition time as a function of the mantle temperature. Here, the oxic transition time is the time at which $P(K_{\text{oxy}} > 1)$ is 95%. Black diamonds represent outputs of the standard case (see also Supplementary Figure 2).



Supplementary Figure 4: Oxygen fugacity of the fayalite-magnetite-quartz buffer as a function of temperature. The $f_{O_2, FMQ}$ is calculated using a function given by [6].

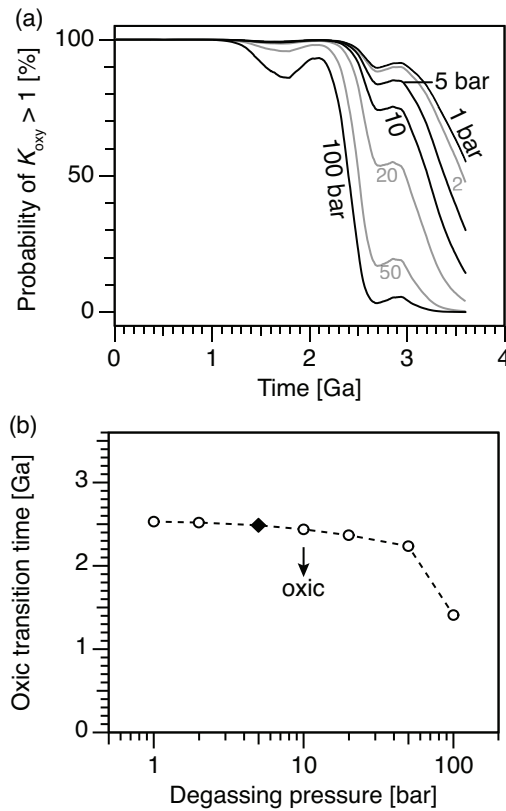
ing temperature [e.g., 7]. However, we have to note that island arc basalts tends to be more oxidized than mid-ocean ridge basalt or oceanic island basalt [8]. Hence, to examine the oxidation effect of the volcanic gas vented from arc volcanoes, we also have to consider the difference in ΔFMQ between the mantle and the volcanic arc.

Comparison with previous study This trend of the oxic transition time with mantle temperature is consistent with [9] but inconsistent with [10]. The main difference of these studies is the assumption of the f_{O_2} of volcanic gas. In [9] and this study, it is assumed that the f_{O_2} of the volcanic gas is buffered by the f_{O_2} of mantle. Hence, cooling results in a decrease in the absolute value of f_{O_2} of the mantle and the volcanic gas, which makes volcanic gas more reducing.

In [10], it is assumed that the volcanic gas is a closed system, i.e., decoupled with its source melt. Under such a condition, cooling causes reduction of SO_2 to H_2S , which is accompanied by oxidation of H_2 to H_2O [10, 9]. Hence, the ratio of H_2O to H_2 in the volcanic gas increases with cooling, resulting in the apparent increase in f_{O_2} of the volcanic gas relative to f_{O_2} of the source melt. However, in a closed system, reduction of one gas must be accompanied by oxidation of another gas because the reduction of SO_2 is accompanied by the oxidation of H_2 . Hence, the overall O_2 sink in the gas mixture does not change [9].

1.2 Degassing pressure

Volcanic gases tend to become more reducing with increasing pressure of degassing. Thus, previous studies [e.g., 11, 12] proposed that a change in volcanic degassing from submarine settings (where the weight of the ocean can add a few 100 bar) to subaerial settings triggered the GOE, though the effect of pressure might be overestimated [13]. Here, we calculated K_{oxy} with different degassing pressure (Supplementary Figure 3) and obtained a similar trend [e.g., 11, 12].



Supplementary Figure 5: A sensitivity study for degassing pressure: (a) $P(K_{\text{oxy}} > 1)$ as a function of time, and (b) an oxic transition time as a function of the pressure. See also Supplementary Figure 3. The $P(K_{\text{oxy}} > 1)$ tends to increase with the decrease in the mantle temperature (a), which is consistent with previous works [e.g. 11, 12].

Supplementary Figure 5a shows the evolutions of $P(K_{\text{oxy}} > 1)$ for differ-

ent pressures of degassing. As shown in Supplementary Figure 5a, higher degassing pressure tends to result in lower $P(K_{\text{oxy}} > 1)$, i.e., smaller K_{oxy} . This trend is consistent with previous works [e.g., 11, 12]. Hence, the oxic transition time becomes smaller in units of Ga (Supplementary Figure 5b).

Thus, a transition from submarine to subaerial volcanism, i.e., a decrease in the degassing pressure, might have played a role in the oxygenation of atmosphere [11], in addition to secular mantle oxidation.

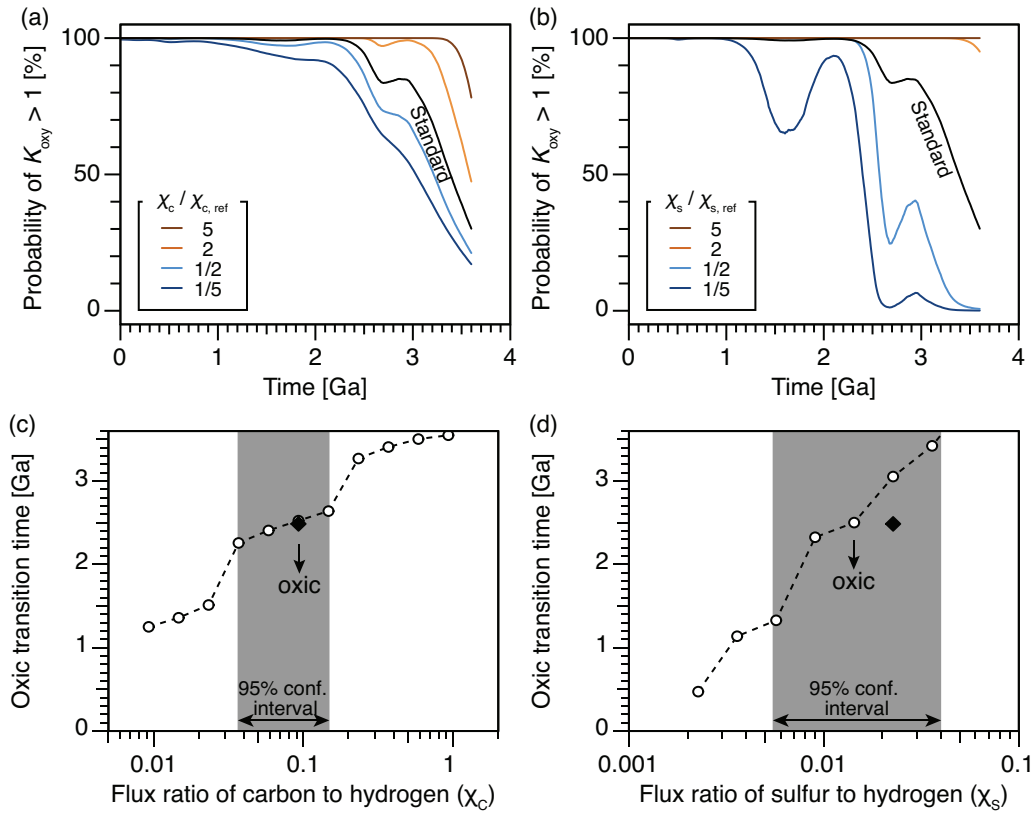
1.3 Total flux ratio of carbon and sulfur

We assumed constant total flux ratios of carbon (χ_c) and sulfur (χ_s) relative to total hydrogen in Eq. (2) for the standard case (Fig. 2), but they may have changed with time. Indeed, [14] assumed that the volcanic recycling of CO_2 and SO_2 increased with time as sedimentary reservoirs of carbon and sulfur grew and suggested that the ratio of $\text{CO}_2/\text{H}_2\text{O}$ and $\text{SO}_2/\text{H}_2\text{O}$ increased with time, which caused the GOE. Here, we examined the effect of (χ_c) and (χ_s) on K_{oxy} (Supplementary Figure 6) and obtained similar trend [14].

Supplementary Figure 6a and 6b show the evolution of $P(K_{\text{oxy}} > 1)$ for (a) different ratios of a total carbon flux to a total hydrogen flux (χ_c) and (b) different ratios of a total sulfur flux to a total hydrogen flux (χ_s). As shown in Supplementary Figure 6a and 6b, higher χ_c (χ_s) tends to result in higher $P(K_{\text{oxy}} > 1)$, i.e., higher K_{oxy} . This is because larger χ_c (χ_s) tends to increase the numerator of Eq. (2). These results are consistent with the suggestion of Holland [14] that larger χ_c ($\sim \text{CO}_2/\text{H}_2\text{O}$) and/or χ_s ($\sim \text{SO}_2/\text{H}_2\text{O}$) tend to favor an oxic atmosphere and could drive the GOE.

Supplementary Figure 6c and 6d show the oxic transition time as a function of (c) χ_c and (d) χ_s . Note that in Supplementary Figure 6c and 6d, black diamonds, which represent the oxic transition time of the standard case, are slightly offset from the dashed lines. This is because for the standard case, we integrated the oxic transition time using the distribution of χ_c and χ_s . The increase in χ_c (χ_s) increases the oxic transition time (Supplementary Figure 6c and 6d) because larger χ_c (χ_s) results in larger K_{oxy} (Supplementary Figure 6a and 6b).

Estimating the evolution of parameters χ_c and χ_s is outside of the scope of this study but may be necessary for understanding of the evolution of Earth's surface oxidation.



Supplementary Figure 6: A sensitivity study for the ratio of a total flux of an element (C or S) to the total flux of hydrogen: a and c are for the total carbon flux to the total hydrogen flux, χ_c , and b and d are for the ratio of the total flux of sulfur to the total flux of hydrogen, χ_s . The gray shaded regions represent the 95% confidence interval of modern values of χ_c (0.1 ± 0.06 [2SD]) and χ_s (0.023 ± 0.017 [2SD]), respectively. See also Supplementary Figure 3.

1.4 Magnetite deposition

The deposition of magnetite via serpentinization works as a sink of oxygen because it generates oxidizable hydrogen (simplified as $3\text{FeO} + \text{H}_2\text{O} \rightarrow \text{Fe}_3\text{O}_4 + \text{H}_2$), although serpentinization is a relatively minor sink today [15, 16]. However, in the Archean, serpentinization rates might have been enhanced by an oceanic crust including a larger amount of olivine. Such crust could have been produced by a higher mantle temperature because the higher mantle temperature would cause a greater degree of partial melting, resulting in an igneous product that is similar to its mantle source [17]. Hence, the deposition of magnetite might affect the redox state of the atmosphere on the Archean Earth [17]. Here, we calculated the K_{oxy} by varying the magnetite deposition flux (Supplementary Figure 7) and obtained a similar conclusion to Kasting [17].

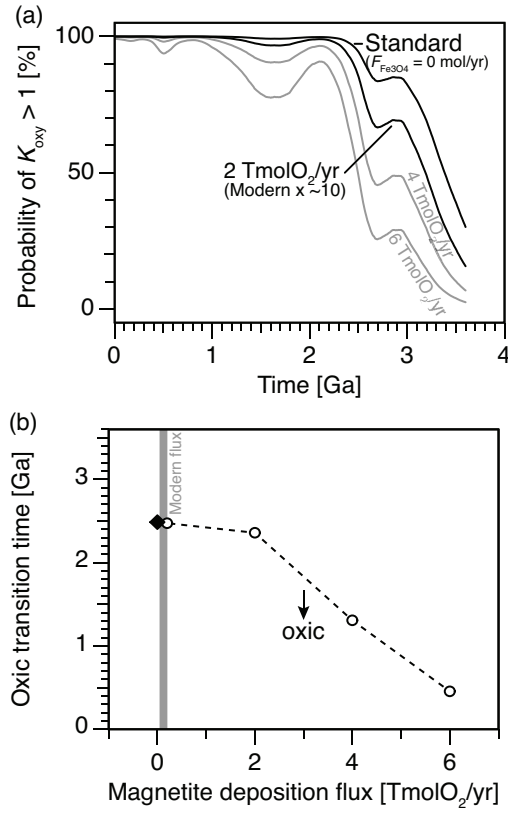
Supplementary Figure 7a shows the evolutions of $P(K_{\text{oxy}} > 1)$ for different fluxes of magnetite deposition. As shown in Supplementary Figure 7a, higher magnetite deposition flux results in lower $P(K_{\text{oxy}} > 1)$, i.e., smaller K_{oxy} .

Supplementary Figure 7b shows the oxic transition time for different fluxes of magnetite deposition. The modern flux of magnetite deposition is estimated to be 0.05 to $\sim 0.2 \text{ TmolO}_2 \text{ yr}^{-1}$ [15, 16], and the range is represented by the gray shaded region in Supplementary Figure 7a. Given the higher mantle potential temperature in the Archean, the oceanic crust would have been thicker and more olivine-rich than today [e.g., 18]. As a result, the flux of magnetite deposition may have been as much as 10 times or more higher than the modern flux ($\sim 2 \text{ TmolO}_2 \text{ yr}^{-1}$) as suggested by [17].

1.5 Oxygen fugacity of the modern mantle

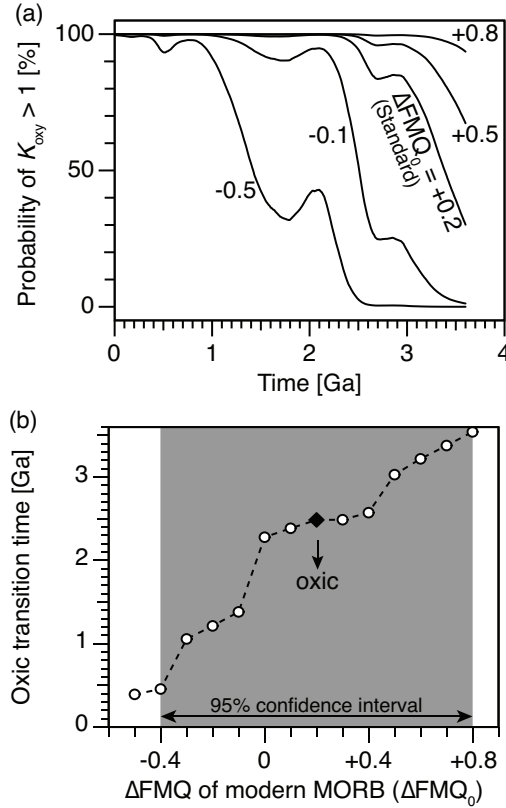
As explained in Supplementary Note 4, we anchor the evolution of oxygen fugacity (f_{O_2}) of the mantle so that at $t = 0 \text{ Ga}$ (now) the average value of f_{O_2} is that inferred for the mantle from mid-ocean ridge basalt (MORB). Hence, the f_{O_2} value chosen for the modern mantle anchors the absolute value of the trend of past f_{O_2} , and therefore affects the calculated trend of K_{oxy} in the past.

For the standard case, we apply the average oxygen fugacity of the modern mantle, which is +0.2 in the \log_{10} unit relative to the fayalite-magnetite-quartz (FMQ) buffer (i.e., $\Delta\text{FMQ}_0 = +0.2$) according to [19]. However,



Supplementary Figure 7: A sensitivity study for deposition flux of magnetite (Fe_3O_4): (a) $P(K_{\text{oxy}} > 1)$ as a function of time, and (b) an oxic transition time as a function of the deposition flux of magnetite. See also Supplementary Figure 3. The gray shaded region represents the range of modern flux of magnetite deposition [$0.05 \sim 0.2 \text{ TmolO}_2 \text{ yr}^{-1}$; 15, 16]. See also Supplementary Figure 3.

ΔFMQ_0 has an uncertainty of $\sigma = 0.3$ in \log_{10} units [19]. Here, we investigated the effect of ΔFMQ_0 on the evolution of K_{oxy} (Supplementary Figure 8).



Supplementary Figure 8: A sensitivity study for the oxygen fugacity of modern mid-ocean ridge basalt: (a) $P(K_{\text{oxy}} > 1)$ as a function of time, and (b) an oxic transition time as a function of the pressure (See also Supplementary Figure 3) The gray shaded region represents the 95% confidence interval of the oxygen fugacity of modern MORB ($\text{FMQ}+0.2 \pm 0.6$ [2SD]) according to [19]. See also Supplementary Figure 3.

Anchoring the f_{O_2} trend to a large ΔFMQ_0 causes higher oxygen fugacity of the mantle throughout the past (Eq. (4)). So, this obviously results in a larger $P(K_{\text{oxy}} > 1)$ (Supplementary Figure 8a) and earlier oxic transition time Supplementary Figure 8b.

Supplementary Note 2: Holland's f number

2.1 Relation between Holland's f number and oxygenation parameter

As discussed in Kadoya et al. [9], the oxygenation parameter, K_{oxy} , of a closed gas mixture does not flip from < 1 to > 1 or vice versa if reactions occur within a closed gas mixture. Also, the same conclusion can be obtained in terms of Holland's f number. This point can be mathematically derived by considering the relation between f and K_{oxy} , as follows.

Holland's f number is calculated as follows [e.g., 20]:

$$\begin{aligned} f &= \frac{F_{\text{H}_2} + (1 - 2f_{\text{org}}) F_{\text{CO}} + (4 - 2f_{\text{org}}) F_{\text{CH}_4} - 2f_{\text{org}} F_{\text{CO}_2} + 3F_{\text{H}_2\text{S}}}{3.5F_{\text{S},\text{all}}} + \frac{1}{3.5} \\ &= \frac{F_{\text{H}_2} + F_{\text{CO}} + 4F_{\text{CH}_4} - 2f_{\text{org}} F_{\text{C},\text{all}} + 3F_{\text{H}_2\text{S}}}{3.5F_{\text{S},\text{all}}} + \frac{1}{3.5}, \end{aligned} \quad (\text{S.1})$$

where F_x represents the flux of a material, x . Note that total carbon flux is $F_{\text{C},\text{all}} (= F_{\text{CO}_2} + F_{\text{CO}} + F_{\text{CH}_4})$, and total sulfur flux is $F_{\text{S},\text{all}} (= F_{\text{SO}_2} + F_{\text{H}_2\text{S}})$. The parameter, f_{org} , is the organic burial fraction, which was set at 0.2 in Holland [20]. In this formulation, we also consider methane flux, F_{CH_4} , for consistency with the oxygenation parameter. Note that degassing of 1 mol CH_4 is equivalent to a source of 4 mol H_2 : $\text{CH}_4 + 2\text{H}_2\text{O} \rightarrow \text{CO}_2 + 4\text{H}_2$.

The oxygenation parameter, K_{oxy} , is calculated as follows [e.g., 21]:

$$K_{\text{oxy}} = \frac{4f_{\text{org}} \times F_{\text{C},\text{all}} + 5F_{\text{SO}_2}}{2F_{\text{H}_2} + 2F_{\text{CO}} + 8F_{\text{CH}_4} + F_{\text{H}_2\text{S}}}. \quad (\text{S.2})$$

Using Eqs. S.1 and S.2 produces following equation:

$$f - 1 = \frac{2f_{\text{org}} F_{\text{C},\text{all}} + 2.5F_{\text{SO}_2}}{3.5F_{\text{S},\text{all}}} \times \left(\frac{1}{K_{\text{oxy}}} - 1 \right). \quad (\text{S.3})$$

Since $F_{\text{C},\text{all}}$, $F_{\text{S},\text{all}}$, F_{SO_2} , and f_{org} are not negative, the sign of $(f - 1)$ is identical with that of $(-1 + 1/K_{\text{oxy}})$; therefore,

$$\begin{cases} f > 1 & \iff K_{\text{oxy}} < 1 \\ f = 1 & \iff K_{\text{oxy}} = 1 \\ f < 1 & \iff K_{\text{oxy}} > 1 \end{cases}. \quad (\text{S.4})$$

The oxygenation parameter, K_{oxy} , of a closed gas mixture does not flip from < 1 to > 1 or vice versa as long as reactions occur within the closed

gas mixture [9]. According to the relation between f and K_{oxy} summarized in Eq. S.4, Holland’s f number of the closed gas mixture also does not flip from > 1 to < 1 or vice versa as long as reactions occur within the closed gas mixture.

2.2 Temperature dependence of Holland’s f number and oxygenation parameter

The temperature dependence of Holland’s f number and K_{oxy} is shown in Fig. 9 and 10.

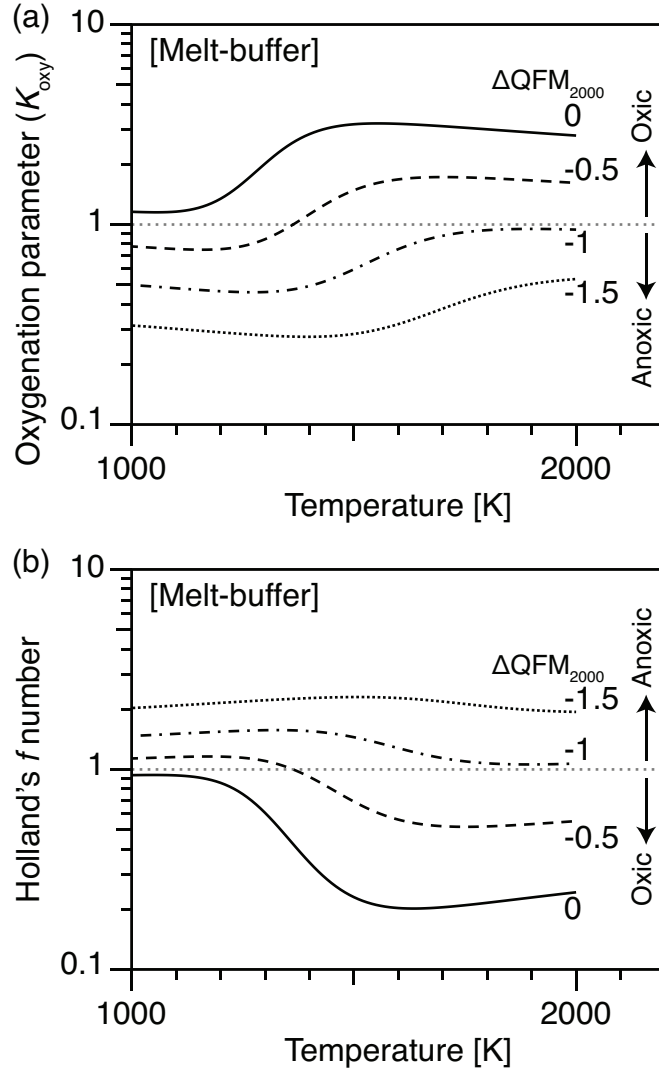
First, assume that the oxygen fugacity of a gas mixture is buffered by that of the ambient melt (i.e., the melt-buffer system in Kadoya et al. [9]). Note that the oxidation state of each case in Fig. 9 is represented by ΔFMQ that is a difference of the logarithm of oxygen fugacity of a gas mixture from that of the fayalite-magnetite-quartz buffer level. For consistency with another case, we represent the oxidation state as ΔFMQ_{2000} that is ΔFMQ at 2000 K. However, we assumed that ΔFMQ of the ambient melt, and therefor of the gas mixture, is constant.

For the melt buffer system, a decrease in temperature tends to decrease K_{oxy} (Fig. 9a). Note that Fig. 9a is the same with Fig. 1b of Kadoya et al. [9]; so for detailed information, see Kadoya et al. [9]. On the other hand, the decrease in temperature tends to increase the f number (Fig. 9a).

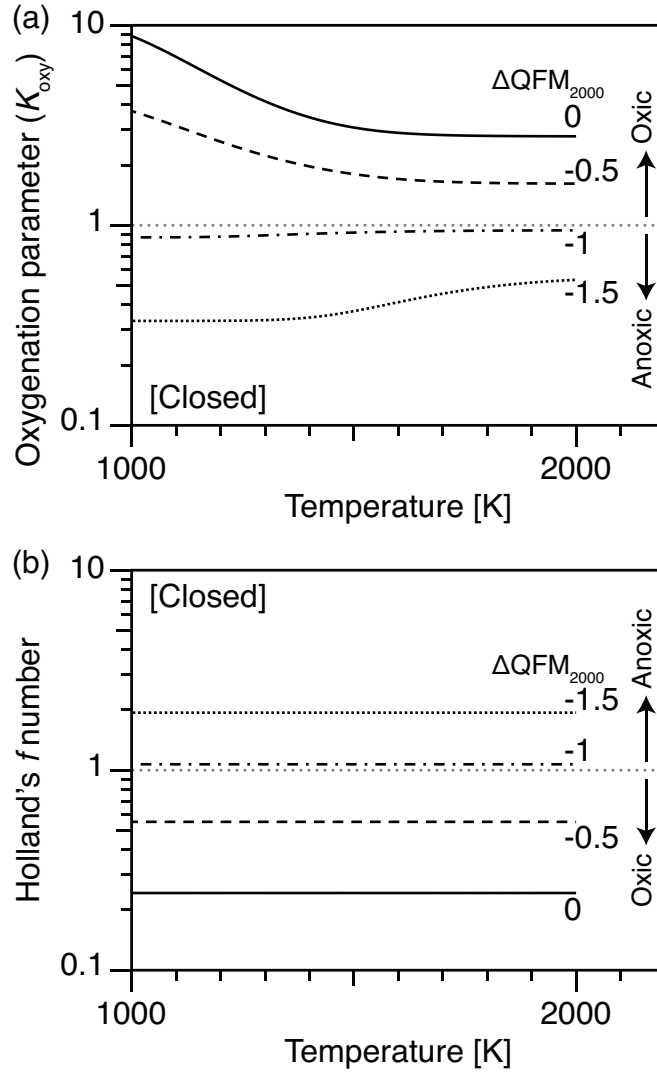
Here, let us focus on the case of $\Delta\text{FMQ}_{2000} = -0.5$ (dashed lines in Fig. 9). As explained in Kadoya et al. [9], K_{oxy} of $\Delta\text{FMQ}_{2000} = -0.5$ shifts from > 1 to < 1 with a decrease in temperature around 1400 K (Fig. 9a). On the other hand, the f number of $\Delta\text{FMQ}_{2000} = -0.5$ shifts from < 1 to > 1 with a decrease in temperature around 1400 K (Fig. 9b). Both of these shifts indicate that the decrease in temperature results in a shift of atmosphere from oxic to anoxic.

Second, consider a closed gas system. For the closed gas system, a decrease in temperature changes K_{oxy} , but K_{oxy} does not flip from < 1 to > 1 or vice versa (Fig. 10a) as explained in Kadoya et al. [9]. Note that Fig. 10a is the same with Fig. 2b of Kadoya et al. [9]. Similarly, the f number does not flip from < 1 to > 1 or vice versa though temperature changes (Fig. 10b). As discussed in Kadoya et al. [9], these results are because of a redox conservation within a closed system.

Thus, temperature dependence of Holland’s f number is essentially same with that of K_{oxy} in terms of redox evolution of the atmosphere.



Supplementary Figure 9: Oxygenation effect of a volcanic gas as a function of temperature.: (a) oxygenation parameter (K_{oxy}), and (b) Holland's f number. The melt-buffer system is assumed (see Fig. 1 of Kadoya et al. [9]). Decrease in temperature results in (a) a decrease in K_{oxy} and (b) an increase in f number. In particular, K_{oxy} of $\Delta\text{FMQ}_{2000} = -0.5$ (dashed lines in a) flips from > 1 to < 1 around 1400 K. Similarly, the f number of $\Delta\text{FMQ}_{2000} = -0.5$ (dashed lines in b) flips from < 1 to > 1 . Both of these lines show that temperature decrease shift atmosphere from oxitic to anoxic if the oxidation state of the melt, and therefore of a volcanic gas, is $\Delta\text{FMQ} = -0.5$. For detailed information, see Kadoya et al. [9].



Supplementary Figure 10: Oxygenation effect of a volcanic gas as a function of temperature.: (a) oxygenation parameter (K_{oxy}), and (b) Holland's f number. The closed system is assumed (see Fig. 2 of Kadoya et al. [9]). Decrease in temperature changes K_{oxy} ; however, K_{oxy} does not flip from < 1 to > 1 or vice versa. Similarly, Holland's f number does not flip from < 1 to > 1 or vice versa. For detailed information, see Kadoya et al. [9].

Supplementary Note 3: Oxygen fugacity of mantle

In this study, we model the evolution of the oxygen fugacity of mantle according to the data of Aulbach and Stagno [22] and Nicklas et al. [23]. As shown in Fig. 1a, these two datasets seem to have similar trends but are offset. In this section, we discuss the similarity and difference between the two datasets by using a linear function. Then, we derive the model of the evolution of the oxygen fugacity of mantle.

3.1 Comparison of trends of two datasets of the oxygen fugacity evolution

First of all, we compare trends of the two datasets using an F test. For a null hypothesis, we assumed that the two datasets are fitted by two linear functions whose slopes are the same but whose intercepts are different from each other: i.e., for the data of Aulbach and Stagno [22],

$$\Delta\text{FMQ} = a_1 t + \Delta\text{FMQ}_{1,\text{AS}}, \quad (\text{S.5})$$

and for the data of Nicklas et al. [23],

$$\Delta\text{FMQ} = a_1 t + \Delta\text{FMQ}_{1,\text{N}}. \quad (\text{S.6})$$

Here, t is in the unit of Ga, and the oxygen fugacity is in \log_{10} units relative to the Fayalite-Magnetite-Quartz (FMQ) buffer. The parameters, a_1 , $\Delta\text{FMQ}_{1,\text{AS}}$, and $\Delta\text{FMQ}_{1,\text{N}}$, are analytically computed to be -0.29 ± 0.05 [2σ] in the unit of [$1/\text{Ga}$], 0.0 ± 0.15 [2σ], and 1.20 ± 0.05 [2σ], respectively. Using these functions, the squared sum of residuals is 96.9.

On the other hand, as an alternative hypothesis, we assumed that the two datasets are fitted by two linear functions whose slopes and intercepts are different from each other: i.e., for the data of Aulbach and Stagno [22].

$$\Delta\text{FMQ} = a_{2,\text{AS}} t + \Delta\text{FMQ}_{2,\text{AS}}, \quad (\text{S.7})$$

and for the dataset of Nicklas et al. [23],

$$\Delta\text{FMQ} = a_{2,\text{N}} t + \Delta\text{FMQ}_{2,\text{N}}. \quad (\text{S.8})$$

Equations S.7 and S.8 are represented by dotted and dashed lines in Fig. 1a, respectively. The parameters for Aulbach and Stagno [22], $a_{2,\text{AS}}$ and $\Delta\text{FMQ}_{2,\text{AS}}$,

are analytically computed to be $-0.41 \pm 0.17 [2\sigma]$ in the unit of $[/Ga]$ and $0.14 \pm 0.24 [2\sigma]$, respectively. Similarly, the parameters for Nicklas et al. [23], $a_{2,N}$ and $\Delta FMQ_{2,N}$, are analytically computed to be $-0.27 \pm 0.05 [2\sigma]$ in the unit of $[/Ga]$ and $1.2 \pm 0.1 [2\sigma]$, respectively. Using these functions, the squared sum of residuals is 94.7.

The number of data is 12 for Aulbach and Stagno [22] and 18 for Nicklas et al. [23]. We use four parameters for the null hypothesis and three parameters for the alternative hypothesis. So, the F-value is calculated as follows:

$$F = \left(\frac{96.9 - 94.7}{(12 + 18 - 3) - (12 + 18 - 4)} \right) \left(\frac{94.7}{12 + 18 - 4} \right)^{-1} \sim 0.61. \quad (S.9)$$

Considering an F distribution with this F-value (0.61), the p-value is calculated to be 44%. Since the p-value is higher than a canonical rejection rate (5%), we cannot reject the null hypothesis. Hence, we consider that the slopes of the fitting functions for the two datasets are the same as each other.

3.2 Comparison of offsets of two datasets of the oxygen fugacity evolution

As explained above, we fit the two datasets by linear functions whose slopes are the same as each other. Then, we compare the intercepts of the linear functions using the F test.

For a null hypothesis, we assumed that the two datasets are fitted by one linear function. The fitting function for both of Aulbach and Stagno [22] and Nicklas et al. [23] is as follows:

$$\Delta FMQ = a_3 t + \Delta FMQ_3. \quad (S.10)$$

The parameters, a_3 and ΔFMQ_3 , are analytically computed to be $-0.21 \pm 0.05 [2\sigma]$ in the unit of $[/Ga]$ and $0.9 \pm 0.1 [2\sigma]$, respectively. Using this function, the squared sum of residuals is 329.3.

On the other hand, for an alternative hypothesis, we assumed that that the two datasets are fitted by two linear functions whose slopes are the same but intercepts are different from each other: i.e., the null hypothesis above (see Eq. S.5 and S.6, and related explanation). As explained above, using Eq. S.5 and S.6, the squared sum of residuals is 96.9.

The number of data is 12 for Aulbach and Stagno [22] and 18 for Nicklas et al. [23], and we use three parameters for the null hypothesis and 2 parameters

for the alternative hypothesis. So, the F-value is calculated as follows:

$$F = \left(\frac{329.3 - 96.9}{(12 + 18 - 2) - (12 + 18 - 3)} \right) \left(\frac{96.9}{12 + 18 - 3} \right)^{-1} \sim 64.8. \quad (\text{S.11})$$

Considering an F distribution with this F-value (64.8), the p-value is calculated to be $1.2 \times 10^{-6}\%$. Since the p-value is lower than the canonical rejection rate (5%), we reject the null hypothesis.

3.3 Oxygen fugacity of the modern mantle

As explained above, the two datasets of the oxygen fugacity (f_{O_2}) evolutions [22, 23] are fitted by linear functions whose slopes are the same but whose intercepts are different. The difference in the absolute values of f_{O_2} is due to the issue of the inter-calibration of different oxybarometers, or due to the difference in mantle melting process between ridge and plume [24, 23].

In this study, we anchor the evolution of the f_{O_2} at the value which is evaluated using the oxidation state of iron in the modern mid ocean ridge (MORB) samples [19]. According to O'Neill et al. [19], the f_{O_2} of the modern MORB is $0.2 \pm 0.6 [2\sigma]$ in \log_{10} units relative to the FMQ buffer. So, for a standard case of this study, we assumed that the oxygen fugacity of the modern mantle is FMQ+0.2. The variation in the modern oxygen fugacity is considered later as a parameter study.

Setting the oxygen fugacity of the modern mantle, we can regard the intercepts calculated above (i.e., $\Delta\text{FMQ}_{1,\text{AS}}$ in Eq. S.5, and $\Delta\text{FMQ}_{1,\text{N}}$ in Eq. S.6) as the offset from the evolution of the oxygen fugacity. For the standard case, the average offset is +0.2 for Aulbach and Stagno [22], and -1.00 for Nicklas et al. [23].

Supplementary References

- [1] Krissansen-Totton, J., Buick, R., & Catling, D. C. A statistical analysis of the carbon isotope record from the Archean to Phanerozoic and implications for the rise of oxygen. *Am. J. Sci.* **315**, 275–316 (2015).
- [2] Herzberg, C., Condie, K., & Korenaga, J. Thermal history of the Earth and its petrological expression. *Earth Planet. Sc. Lett.* **292**, 79–88 (2010).
- [3] Holland, H. D. *The Chemical Evolution of the Atmosphere and Oceans*. (Princeton University Press, Princeton, 1984).
- [4] Nisbet, E. G., Cheadle, M. J., Arndt, N. T., & Bickle, M. J. Constraining the potential temperature of the Archean mantle - a review of the evidence from komatiites. *Lithos* **30**, 291–307 (1993).
- [5] Aulbach, S. & Arndt, N. T. Eclogites as palaeodynamic archives: Evidence for warm (not hot) and depleted (but heterogeneous) Archaean ambient mantle. *Earth Planet. Sc. Lett.* **505**, 162–172 (2019).
- [6] Wones, D. R. & Gilbert, M. C. The fayalite-magnetite-quartz assemblage between 600 and 800 c. *Am. J. Sci.*, 267:480–488, 1969.
- [7] Till, C. B., Grove, T. L., & Withers, A. C. The beginnings of hydrous mantle wedge melting. *Contrib. Mineral. Petr.* **163**, 669–688 (2012).
- [8] Carmichael, I. S. E. The redox states of basic and silicic magmas: a reflection of their source regions? *Contrib. Mineral. Petr.* **106**, 129–141 (1991).
- [9] Kadoya, S., Catling, D. C., Nicklas, R. W., Puchtel, I. S., & Anbar, A. D. Mantle cooling causes more reducing volcanic gases and gradual reduction of the atmosphere. *Geochem. Perspec. Lett.* **13**, 25–29 (2020).
- [10] Moussallam, Y., Oppenheimer, C., & Scaillet, B. On the relationship between oxidation state and temperature of volcanic gas emissions. *Earth Planet. Sc. Lett.* **520**, 260–267 (2019).
- [11] Kump, L. R. & Barley, M. E. Increased subaerial volcanism and the rise of atmospheric oxygen 2.5 billion years ago. *Nature* **448**, 1033–1036 (2007).

- [12] Gaillard, F., Scaillet, B., & Arndt, N. T. Atmospheric oxygenation caused by a change in volcanic degassing pressure. *Nature* **478**, 229–233 (2011).
- [13] Brounce, M., Stolper, E., & Eiler, J. Redox variations in mauna kea lavas, the oxygen fugacity of the hawaiian plume, and the role of volcanic gases in Earth’s oxygenation. *P. Natl. Acad. Sci. USA* **114**, 8997–9002 (2017).
- [14] Holland, H. D. Why the atmosphere became oxygenated: A proposal. *Geochim. Cosmochim. Ac.* **73**, 5241–5255 (2009).
- [15] Sleep, N. H. Dioxygen over geologic time. in *Metal Ions in Biological Systems, Vol. 43, Biogeochemical Cycles of Elements* (eds. Sigel, H. & Sigel, R.) 49–73 (Taylor & Francis, Boca Raton, FL 2005).
- [16] Canfield, D. E., Rosing, M. T., & Bjerrum, C. Early anaerobic metabolisms. *Philos. T. R. Soc. B.* **361**, 1819–1834 (2006).
- [17] Kasting, J. F. What caused the rise of atmospheric O₂? *Chem. Geol.* **362**, 13–25 (2013).
- [18] Sleep, N. H. Evolution of the Earth: Plate tectonics through time. in *Treatise on Geophysics (Second Edition)* (eds. Schubert, G.) 145–172 (Elsevier, Oxford, 2015).
- [19] O’Neill, H. S. C., Berry, A. J., & Mallmann, G. The oxidation state of iron in mid-ocean ridge basaltic (MORB) glasses: Implications for their petrogenesis and oxygen fugacities. *Earth Planet. Sc. Lett.* **504**, 152–162 (2018).
- [20] Holland, H. D. Volcanic gases, black smokers, and the Great Oxidation Event. *Geochim. Cosmochim. Ac.* **66**, 3811–3826 (2002).
- [21] Catling, D. C. & Claire, M. W. How Earth’s atmosphere evolved to an oxidic state: A status report. *Earth Planet. Sc. Lett.* **237**, 1–20 (2005).
- [22] Aulbach, S. & Stagno, V. Evidence for a reducing Archean ambient mantle and its effects on the carbon cycle. *Geology* **44**, 751–754 (2016).

- [23] Nicklas, R. W. et al. Secular mantle oxidation across the Archean-Proterozoic boundary: Evidence from V partitioning in komatiites and picrites. *Geochim. Cosmochim. Ac.* **250**, 49–75 (2019).
- [24] Mallmann, G. & O’Neill, H. S. Calibration of an empirical thermometer and oxybarometer based on the partitioning of Sc, Y and V between olivine and silicate melt. *J. Petrol.* **54**, 933–949 (2013).